Sustainable Cities and Society 131 (2025) 106671

Contents lists available at ScienceDirect

Sustainable Cities and Society

journal homepage: www.elsevier.com/locate/scs

Heat wave risk assessment in Bologna using Spatio-temporal artificial intelligence: Leveraging LSTM enhanced by the hippopotamus optimization algorithm

Aniseh Saber [a], Claudia De Luca [a], Ali Pourzangbar [b,*], Simona Tondelli [a], Michelle L. Bell [c]

[a] Department of Architecture, Alma Mater Studiorum, University of Bologna, Bologna, Italy
[b] Institute for Water and Environment, Karlsruhe Institute of Technology, Karlsruhe, Germany
[c] Yale School of the Environment, Yale University, New Haven, USA

ARTICLE INFO

Keywords:
Heat wave Risk Assessment
LSTM
Older Population
Machine Learning
Bologna

ABSTRACT

This study proposes a spatio-temporal machine learning framework that integrates a Long Short-Term Memory network with the nature-inspired Hippopotamus Optimization Algorithm for Heat Wave Risk (HWR) assessment in Bologna, Italy, where HWR refers to the combined threat posed by the intensity, frequency, and duration of extreme heat events and their impact on exposed and vulnerable populations. We utilized environmental, infrastructure, and demographic data spanning from 2014 to 2023. The heat wave model was developed using 14 key factors covering hazard, exposure, and vulnerability under Representative Concentration Pathways (RCPs) 4.5, 6.0, and 8.5. Inspection of the results revealed temperature, distance to public transportation, local climate zone, and Enhanced Vegetation Index (EVI) as critical factors influencing HWR. Performance evaluations employing statistical indices and a confusion matrix affirm the model's robust predictive capabilities. The developed model accurately distinguished between risk categories, achieving class-wise accuracies of 77.76 % for the 'Very Low' risk class and 78.72 % for the 'High' risk class, both of which were considered satisfactory. The Partial Dependence Plot approach is employed to interpret the behavior of the developed machine learning model, revealing that high temperatures, high relative humidity, limited vegetation cover, and increased distance from critical services such as healthcare and public transportation strongly influence the predicted HWR. Notably, projections under RCP 8.5 predict a significant increase in 'Very High' risk areas from 34 % in 2023 to 65 % by 2050. The study also confirms that enhancements in EVI and reduced proximities to green areas significantly mitigate HWR. These results emphasize the importance of incorporating targeted green infrastructure in urban planning to enhance resilience against heat waves, providing essential insights for urban planners and policymakers.

1. Introduction

Heat waves, defined as prolonged periods of abnormally high temperatures, have become one of the most critical and deadly manifestations of climate change. The Intergovernmental Panel on Climate Change (IPCC, 2023) projects that urban areas in Europe may experience temperature increases between 2 and 8 °C by the end of the 21st century. These conditions are expected to intensify the frequency, duration, and severity of heat waves (Vicedo-Cabrera et al., 2023). Numerous studies have demonstrated consistent associations between heat waves and adverse health outcomes (Anderson & Bell, 2011; Gasparrini et al., 2015). From 2000 to 2019, nearly 489,000 heat-related deaths have been recorded annually, with Europe bearing a disproportionate burden (Lhotka & Kyselý, 2022). Notable events such as the 2003 European heat wave, which caused over 70,000 fatalities (Ballester et al., 2023), and the record-breaking temperatures in 2023 underscore the urgent need for accurate and actionable Heat Wave Risk (HWR) assessments.

To understand the impact of heat waves on human health and well-being, it is essential to analyze both the spatial distribution and temporal evolution of heat waves, as these characteristics vary by region and over time. Urban areas are particularly vulnerable to heat waves due to the Urban Heat Island (UHI) effect, where built environments absorb and retain heat, exacerbating temperature extremes (Gao et al., 2019). These

* Corresponding author.
E-mail address: ali.pourzangbar@kit.edu (A. Pourzangbar).

https://doi.org/10.1016/j.scs.2025.106671
Received 20 April 2025; Received in revised form 19 July 2025; Accepted 19 July 2025
Available online 25 July 2025

effects are compounded in cities with aging populations, where residents aged 65 and older are at greater risk due to reduced thermoregulation, pre-existing health conditions, and mobility constraints (Woodland et al., 2023a). Notably, older populations not only face higher exposure but also influence policy development, as municipalities with a higher share of elderly residents are more likely to adopt climate adaptation measures (Yang et al., 2021). This underscores the importance of integrating demographic equity into heat resilience planning. International frameworks such as the Sendai Framework for Disaster Risk Reduction (UNDRR, 2015), the Sustainable Development Goals (SDGs), and the Paris Agreement emphasize the need for comprehensive risk assessments that address the interconnected elements of hazard, exposure, and vulnerability.

Despite advancements, many existing approaches remain limited by three critical issues: (1) oversimplification of complex, nonlinear climate–urban–demographic interactions; (2) lack of interpretability in predictive models; and (3) inadequate forecasting capacity for future climate conditions. As a result, there is a growing demand for integrative, interpretable, and dynamic models capable of supporting localized risk reduction strategies. This study responds to that demand by proposing a spatio-temporal Machine Learning (ML)-based framework that combines a Long Short-Term Memory (LSTM) neural network with the Hippopotamus Optimization Algorithm (HOA) to model HWR in Bologna, Italy. Our approach integrates high-resolution environmental, demographic, and infrastructural data across 10 years (2014–2023) and evaluates projected risks for the year 2050 under three Representative Concentration Pathways (RCPs): 4.5, 6.0, and 8.5.

This study is guided by three key research questions. First, it investigates the extent to which environmental, infrastructural, and demographic indicators contribute to HWR in urban contexts. Second, it explores how effectively a deep learning model, specifically LSTM, optimized using a metaheuristic algorithm can predict HWR at a fine spatial resolution. Third, it examines the role of green infrastructure, particularly urban vegetation, in mitigating future HWR under different climate change scenarios.

To address these questions, the study aims to achieve several objectives. It seeks to develop a comprehensive, data-driven HWR index that incorporates the three dimensions defined by the IPCC: hazard, exposure, and vulnerability. The LSTM model is trained on a ten-year dataset and optimized using the HOA to improve prediction accuracy and generalization. To enhance interpretability, the study applies Partial Dependence Plots (PDPs), allowing for the assessment of each predictor's influence on model outputs. Furthermore, the model forecasts the spatial distribution of HWR in the year 2050 under three climate scenarios—RCP 4.5, RCP 6.0, and RCP 8.5. Lastly, the study evaluates the effectiveness of Nature-Based Solutions (NBS), such as green space density and vegetation coverage, in reducing projected HWR, offering insights for adaptive urban planning.

This study is organized as follows: Section 2 presents a concise literature review of previous research on HWR assessment. Section 3 describes the study area and outlines the definitions of heat wave hazard, exposure, and vulnerability. It also details the data preprocessing steps, the architecture of the LSTM model, the hyperparameter optimization using the HOA algorithm, and the model validation approach. Section 4 presents the results, including model performance, risk mapping, and scenario projections under different RCPs. Section 5 discusses the key findings, as well as the strengths and limitations of the study. Finally, Section 6 summarizes the main conclusions and suggests directions for future research.

2. Literature review

Heat wave risk assessments have traditionally relied on three primary approaches: statistical modeling, process-based simulations, and scenario-based planning.

Statistical models such as linear regression, logistic regression, and generalized additive models have been used to analyze historical climate and health data (Mudelsee, 2019). These models are relatively simple and interpretable but often fail to capture the nonlinear and spatio-temporal complexity of heat wave impacts, especially in urban environments. Composite indices based on Principal Component Analysis (PCA) or the IPCC risk framework have been used to integrate variables like temperature, age, income, and service access (Sahani et al., 2024; Wang et al., 2023; Wu et al., 2024). These indices can effectively identify high-risk zones but may overlook dynamic interactions between variables.

Process-based models, including land–atmosphere coupled simulations and regional climate models, offer a more physically realistic representation of heat wave dynamics. They incorporate detailed input parameters like land surface temperature, urban morphology, and bioclimatic indices (Varquez et al., 2025). However, their application is limited by high computational cost and data demands. Moreover, they often lack integration with social or health indicators, which are critical for vulnerability assessment.

Scenario-based planning helps in evaluating long-term adaptation pathways under different climate, demographic, and policy scenarios (Gordon & Glenn, 2003; Shah & Sharifi, 2025). This method is valuable for strategic planning but lacks predictive accuracy and operational utility. Limitations include weak integration of health data, inconsistent indicators, and limited contextual sensitivity (Ye & Yang, 2025).

Recent advances have increasingly embraced Artificial Intelligence (AI) and ML approaches. ML models can uncover nonlinear patterns across large and heterogeneous datasets (Reichstein et al., 2019), offering improved accuracy and granularity. In recent years, a wide range of ML model configurations have been effectively employed for climate risk modeling. These include neural network-based approaches such as Convolutional Neural Networks (CNNs) (Jacques-Dumas et al., 2022), Deep Neural Networks (DNNs) (Yadav & Thakkar, 2024), Recurrent Neural Networks (RNNs) (Byagar et al., 2024), and LSTM networks (Chung et al., 2020). Kernel-based models, particularly Support Vector Machines (SVMs) (Khan et al., 2021; Pourzangbar et al., 2017a), as well as ensemble learning techniques such as Categorical Boosting (Pourzangbar et al., 2025; Razavi-Termeh et al., 2025), Gradient Boosting (Ghafarian et al., 2022), and Random Forests (Kumar et al., 2021), have also demonstrated significant success in capturing the complex patterns associated with climate-related hazards. Yet, the performance of ML models is highly sensitive to hyperparameter tuning, which can lead to convergence issues or overfitting (Dhake et al., 2023). To compensate for this limitation, ML models are integrated with metaheuristic algorithms. Various methods, including local and global optimization techniques, are employed to tune these parameters. Recently, various types of metaheuristic algorithms including Imperialist Competitive Algorithm (Nur et al., 2022), Whale Optimization Algorithm (García-Nieto et al., 2021), Grey Wolf Optimizer (Rezaie et al., 2022), Grid Search (Ahmadlou et al., 2022), Particle Swarm Optimization (PSO) (Kumar et al., 2019), Genetic Algorithm (GA) (Karimi et al., 2024), Differential Evolution (Zeng et al., 2022), and Grasshopper Optimization Algorithm (Han & Vartosh, 2023) have been successfully integrated with ML algorithms to map climate-induced hazard and risk susceptibility. However, the application of integrated ML models in HWR mapping is limited. Most studies have focused on isolated components of HWR, primarily vulnerability, rather than conducting comprehensive risk assessments.

LSTM networks are particularly well-suited for time-series analysis due to their ability to capture long-term dependencies (Chung et al., 2020). This has led to the adoption of metaheuristic algorithms to enhance performance. Compared to traditional algorithms such as PSO, which updates solutions based on swarm dynamics, and GA, which depend on crossover and mutation operations, the HOA algorithm achieves a more effective balance between exploration and exploitation, reducing the risk of premature convergence and making it ideal for optimizing deep learning models in high-dimensional, nonlinear

problems (Pavlov-Kagadejev et al., 2024). Moreover, HOA's territory-based strategy and adaptive escape mechanisms enhance population diversity, further improving optimization performance (Amiri et al., 2024).

Despite these advances, model interpretability remains a key challenge (Pourzangbar et al., 2023b). Tools like layer-wise relevance propagation (Bach et al., 2015), gradient-weighted class activation mapping (Selvaraju et al., 2020), Shapley Additive Explanations (SHAP) (Rasheed et al., 2022), as well as PDP (Moosbauer et al., 2021) help reveal the contribution of each feature to the model's predictions. Yet, few studies have applied these techniques in HWR modeling, particularly within spatiotemporal ML-based frameworks.

Therefore, this study aims to bridge these gaps by integrating LSTM with HOA into a spatiotemporal ML-based pipeline for comprehensive heat wave risk assessment. It further applies PDPs to make the model interpretable and aligns the analysis with nature-based mitigation strategies (Chausson et al., 2020; Marando et al., 2022).

3. Material and methods

3.1. Study area

Bologna (44.498955°N; 11.327591°E), located in Italy's Emilia-Romagna region between the Tuscan-Emilian Apennines and the Po Valley, is particularly vulnerable to extreme heat due to its unique geographic and climatic conditions. Its humid subtropical climate and frequent high-pressure systems contribute to intense and prolonged summer heat waves, as well as periods of heavy rainfall and drought (Kottek et al., 2006). Situated within the highly polluted areas (namely, Pianura Padana) (EEA, 2023), and characterized by significant soil consumption, especially in the city center, Bologna presents a critical setting for examining the susceptibility to UHI effects, particularly during the frequent and intense summer heat waves (Cremonini et al., 2023).

Covering an area of 140.9 km^2 and home to approximately 400,000 residents, with a density of 2772 people/km^2, Bologna includes a diverse population of 330,800 Italians and 59,718 foreigners (ISTAT, 2024). The city has been proactive in climate change adaptation (LIFEGATE, 2023), implementing initiatives aligned with the United Nations SDGs and the Sustainable Energy and Climate Action Plan (SECAP) (C40 Cities, 2016), which include enhancing green spaces to mitigate heat effects (Joe et al., 2021). Despite these efforts, Bologna continues to face significant challenges from increasing heat wave intensity and frequency, which disproportionately affects its aging population. The administrative structure—comprising six districts, 18 zones, and a further subdivision into 90 census tracts, as illustrated in Fig. 1—provides a detailed framework for targeted HWR assessment and evaluation of urban planning interventions. Bologna's case underscores the urgent need for ongoing refinement of adaptation strategies to protect its vulnerable populations and enhance overall urban resilience against climatic shifts (Cremonini et al., 2023).

3.2. Methodological approach

This study proposes an integrated spatio-temporal ML-based framework to assess HWR in Bologna, Italy, by combining environmental, meteorological, and socioeconomic data spanning 2014–2023. As outlined in Fig. 2, the methodology comprises three main stages: (1) data collection, (2) preprocessing and model development, and (3) model deployment. Data collection was guided by the IPCC's risk assessment framework, which defines risk in terms of three key components: hazard, exposure, and vulnerability (IPCC, 2014a).

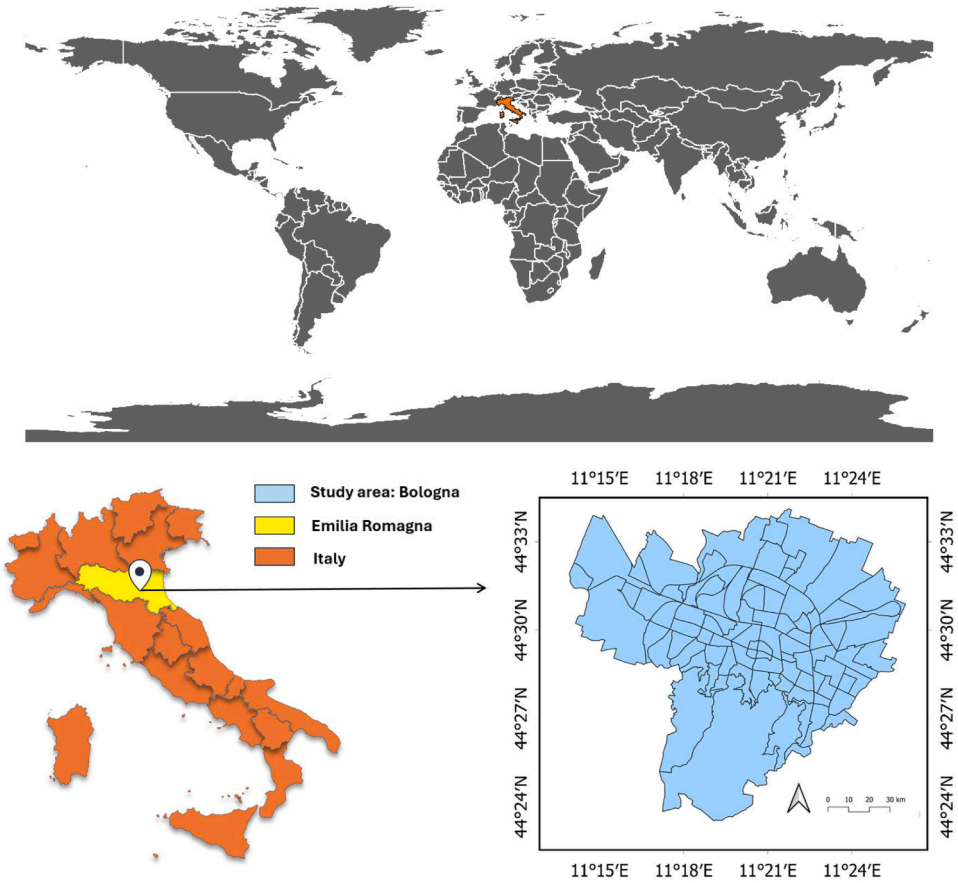

Fig. 1. Boundaries of Bologna metropolitan city: capital of the Emilia-Romagna region in Italy.

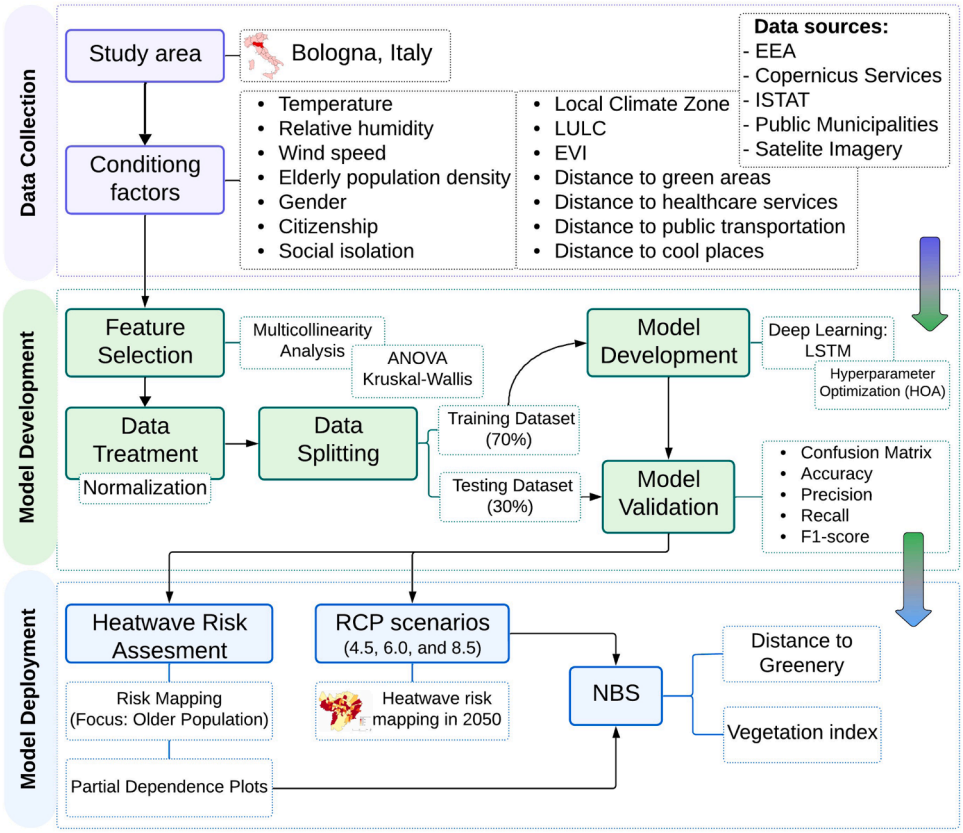

Fig. 2. The block diagram of the proposed methodology: the step-by-step process.

We first gathered a wide range of datasets corresponding to these components such as temperature records (for hazard), demographic and land-use data (for exposure), and socio-economic indicators (for vulnerability). To assess the hazard component, we needed to identify heat wave events. Although there is no universally agreed-upon definition of a heat wave, we adopted a widely used climatological approach: a heat wave is defined as a period during which daily temperatures exceed the 95th percentile of historical summer temperatures for at least three consecutive days (Varghese et al., 2019). This definition enabled us to objectively determine the occurrence and characteristics of heat wave events throughout the study period.

During preprocessing, we applied feature selection to identify relevant predictors and perform multicollinearity analysis to reduce redundancy. The cleaned dataset was split into training and testing subsets to ensure unbiased model evaluation. An LSTM network was employed to predict HWR across spatial units in Bologna. To optimize the model's performance, we used the HOA, a recent metaheuristic designed for efficient hyperparameter tuning. The effectiveness of the developed model was assessed using both statistical metrics (e.g., class-wise accuracy) and visual tools.

3.3. Identification of heat waves

Heat waves are defined variably across disciplines (Becker et al., 2022), adapting to local climates and influenced by international guidelines like those from the World Meteorological Organization (WMO) and World Health Organization (WHO) (WMO & WHO, 2015), which broadly characterizes a heat wave as a period where daily peak temperatures exceed the usual maximum by at least 5 °C for five consecutive days. These guidelines broadly define heat waves by their duration, geographic coverage, and intensity (McCarthy et al., 2019). Nationally, definitions vary: some regions define heat waves by a minimum of three consecutive nights with temperatures above 25 °C, emphasizing the impact on human health and comfort. The United States Environmental Protection Agency (EPA: https://www.epa.gov/) defines a heat wave as at least three or more consecutive days when a city's daily minimum apparent temperature surpasses the 85th percentile of typical summer values. Globally, thresholds differ, with Lisbon recognizing temperatures above 29 °C as hazardous, whereas South Korea and China set higher thresholds of >33 °C and >35 °C, respectively (Park et al., 2020; Wang et al., 2017). Other definitions consider exceedances of the 95th percentile of daily maximum temperatures for at least three consecutive days (Smith et al., 2013). The Australian Bureau of Meteorology describes heat waves as periods lasting at least three days during which both maximum (daytime) and minimum (nighttime) temperatures are unusually high for a specific location, while Italy's Alert System defines them as three consecutive days with maximum temperatures over 30 °C (Nardino et al., 2022). In this study, a heat wave is defined as a period of three or more consecutive days during which daily temperatures exceed the 95th percentile of summer temperatures (June, July, and August), based on a reference period from 2014 to 2023 (Varghese et al., 2019).

3.4. Components of heat wave risk assessment

Risk assessment is a structured process that evaluates the combined influence of three key components: hazard, exposure, and vulnerability as detailed in Fig. 3. This process involves analyzing potential hazards (i.e., heat waves), the exposure of people and assets to these hazards, and their vulnerability, which depends on factors such as socioeconomic status, structural integrity, and preparedness. These elements are crucial for developing innovative strategies to mitigate climate risks.

In this framework (as shown in Fig. 3), each map refers to a spatial representation of a specific risk component across the study area. A hazard map displays the geographic distribution of extreme heat events, considering the frequency, intensity, or duration of heat waves based on

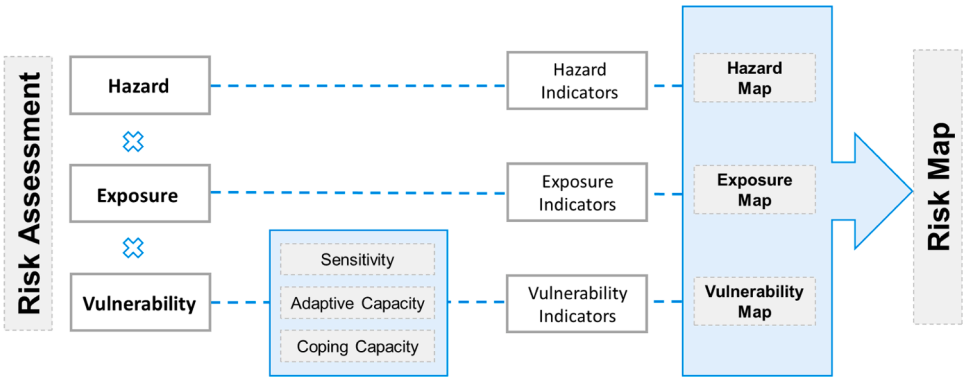

Fig. 3. Framework for risk assessment incorporating Hazard, Exposure, and Vulnerability components.

historical or projected data. An exposure map identifies where populations, infrastructure, or other assets at risk are located, often using population density or land use data. A vulnerability map visualizes regions with higher susceptibility to adverse impacts based on social, economic, and demographic factors, such as age, income, or healthcare access. These individual layers are combined to generate a risk map, which integrates the three components to highlight areas of highest HWR, guiding prioritization for adaptation and mitigation planning.

This study follows the IPCC's widely accepted risk assessment framework, which defines climate risk as a function of hazard, exposure, and vulnerability (i.e., Risk = Hazard × Exposure × Vulnerability) (IPCC, 2014b). This model has been effectively applied in different urban heat risk studies (Aubrecht & Özceylan, 2013), making it well-suited for assessing HWR in complex urban environments. This tripartite structure allows for a comprehensive evaluation of risk by capturing not only the climatic hazard (e.g., heat wave intensity, duration, frequency) but also the spatial distribution of affected populations (exposure) and their capacity to respond or adapt (vulnerability). The specific formula adopted integrates these three components in a normalized (scaled between 0 and 1) and multiplicative form, which ensures that areas with high risk are those where all three dimensions align (e.g., high hazard, high exposure, and high vulnerability). This approach is particularly suitable for urban HWR assessment, as it highlights systemic vulnerabilities in densely populated areas with limited adaptive infrastructure. Moreover, the use of a data-driven modeling approach enhanced by spatiotemporal ML-based modeling ensures flexibility and scalability to other cities or regions.

3.4.1. Hazard

In assessing the risk associated with heat waves, the Heat wave Hazard Index (HHI) considers several critical components (Perkins et al., 2012): Heat Wave Intensity (HWI), Heat Wave Duration (HWD), Heat Wave Frequency (HWF). The HWI was assessed by examining the 95th percentile of temperatures during the summer months using a decade of historical data from 2014 to 2023, which helps analyze the highest extremes of local temperature patterns. The HWD tracks the length of these events, focusing on periods where temperatures exceed this threshold for three or more days, highlighting prolonged risk periods. The HWF, defined as the number of discrete heat wave events occurring within a given year, was explicitly included in the calculation of the heat wave hazard index, along with intensity and duration. This inclusion reflects the essential role of frequency in capturing cumulative exposure. For example, given the same intensity and duration, a location experiencing four heat wave events annually is subject to a higher hazard than one experiencing only two. This aligns with findings by Perkins et al. (2012) and Vivo et al. (2022), who highlight the increasing frequency of heat waves as a significant factor in hazard and risk assessment.

The HHI was calculated by normalizing these components to a scale from 0 to 1 using min-max normalization method (c.f. Section 2.7), ensuring equal contribution to the index regardless of their original measurement scales. The normalized values were then multiplied to compute the overall HHI (Eq. (1)), providing a comprehensive measure of HWR.

$$HHI = HWI_N \times HWF_N \times HWD_N \tag{1}$$

where the subscript N denotes the normalized form of the different components, scaled between 0 and 1.

3.4.2. Exposure

Exposure in risk assessment refers to the presence of vulnerable elements like people, property, and natural resources in hazard-prone areas (Turner et al., 2012). This study assessed exposure by focusing on populations most affected by heat waves, analyzing their spatial distribution and density, especially in European urban centers where the UHI effect significantly exacerbates local temperatures, impacting dense populations of older population residents aged 65 and over (Ellena et al., 2023). These older population groups are considered highly exposed to heat waves (Woodland et al., 2023). The Heat wave Exposure Index (HEI) was calculated by integrating the density of the older population (Eq. (2)) to identify areas where heat waves could have the most direct impact.

$$HEI = \frac{E_i}{P_i} \tag{2}$$

in which E_i is the number of older populations per each census tract i, P_i stands for total populations per census tract.

3.4.3. Vulnerability

In accordance with the IPCC framework, Heat wave Vulnerability Index (HVI) in our study is defined as a function of Sensitivity (S) and Adaptive Capacity (AC). These components were quantified using specific indicators. Sensitivity included demographic and spatial factors such as gender imbalance, the proportion of older adults with a migrant background, elderly individuals living alone, and Local Climate Zones (LCZs). Adaptive Capacity was assessed through access-related indicators, including the proximity to healthcare facilities, green areas, public transportation, cooling shelters, other public cooling spaces, and Enhanced Vegetation Index (EVI). To ensure conceptual consistency, AC was normalized inversely, meaning that higher adaptive capacity resulted in lower vulnerability scores. As a result, areas with strong AC contribute to a reduction in overall vulnerability, and therefore, lower risk when combined with hazard and exposure. The HVI calculation normalized S and AC indicators on a scale from 0 to 1 for consistent comparison across metrics. Each component was weighed equally in our methodology to simplify the quantification of overall vulnerability, avoiding any single factor disproportionately influencing the index. The HVI formula combines these elements (Eq. (3)), ensuring a balanced

assessment of heat wave vulnerability.

$$HVI_i = \frac{1}{2}\left(\frac{1}{n}\sum_{j=1}^{n} S_{ij}\right) + \frac{1}{2}\left(\frac{1}{m}\sum_{k=1}^{m} AC_{ik}\right) \quad (3)$$

HVI_i is Heat wave Vulnerability Index for census tract i, S_{ij} represents the normalized value of the j-th sensitivity indicator in tract i, AC_{ik} is normalized value of the k-th adaptive capacity indicator in tract i, n and m are representing the number of sensitivity indicators and the number of adaptive capacity indicators, respectively.

3.5. Contributing parameters

The study covers a ten-year period (2014–2023), with a focus on the peak temperature of summer months including June, July, and August in Bologna. All variables were calculated as average values over the summer months (June–August), which correspond to the typical heat wave season. It utilized census tracts, which represent the most detailed spatial data available in Italy. The HWR assessment in this study incorporated a diverse set of 14 climatological, demographic, socio-economic, and environmental indicators. Among the hazard indicators are temperature, representing the daily average heat stress and elevated air temperatures exceeding regional climatic norms; relative humidity, which affects the perceived temperature and thermal discomfort; and wind speed, influencing the dispersion of heat and urban ventilation and cooling effects during hot conditions. The exposure component included older population density within each census tract, capturing the concentration of individuals aged 65 and above who are particularly vulnerable to extreme heat.

Given vulnerability, the study considered both S and AC. Sensitivity indicators included gender, the proportion of women aged 65 and over out of the total number of people aged 65 and over, as women are generally more physiologically susceptible to heat-related illness (Bell et al., 2008); citizenship, which accounts for foreign-born older populations who may face barriers to healthcare and support services (Messeri et al., 2019); and social isolation, representing older population individuals living alone and thus at greater risk during heat emergencies (Cianconi et al., 2020). While foreign citizenship is not inherently associated with social isolation, prior studies have shown that older foreign-born populations may face structural barriers (e.g., language, healthcare access, or weaker social networks) that elevate heat-related vulnerability (Ellena et al., 2023). In our analysis, foreign citizenship is treated as a potential vulnerability factor, separate from direct indicators of social isolation, such as elderly individuals living alone. LCZ indicators, which classify urban morphology and its effect on microclimate and heat retention, were used to characterize urban form and land cover features relevant to heat exposure and vulnerability. Specifically, the sky view factor reflects urban canyon geometry, influencing radiative heat trapping and therefore exposure levels. Floor area ratio and building height serve as proxies for urban density, which can exacerbate heat retention and reduce ventilation, increasing vulnerability. In the context of surface characteristics, impervious surfaces (e.g., asphalt, concrete) are associated with higher heat storage capacity and reduced evapotranspiration, thereby increasing vulnerability. In contrast, permeable surfaces (e.g., vegetation, soil) support cooling through evapotranspiration and shading, and are therefore considered part of AC. These classifications are grounded in established urban climate studies (Stewart & Oke, 2012), which link LCZ typologies to differential thermal behavior and urban heat risk profiles. Furthermore, Land Use and Land Cover (LULC), which indicates the dominant surface types such as vegetation, buildings, or water bodies that influence urban heat dynamics is also considered a contributing parameter in the evaluation of HWV. Indicators related to AC include the EVI, reflecting the density and health of vegetation, which provides natural cooling; proximity to green areas, highlighting accessibility to vegetated public spaces; distance to healthcare services, which affects emergency response and access to treatment; distance to public transportation, essential during evacuation or medical needs; and distance to cool places, representing accessibility to designated cooling centers or air-conditioned public facilities. To account for spatial heterogeneity across census tracts, proximity to green spaces was calculated using buffer zones at 100 m, 300 m, and 500 m intervals, representing varying levels of accessibility. For other amenities such as health centers, roads, and public transport, Euclidean distances were computed from the centroid of each census tract to the nearest amenity. This standardization ensures consistency across districts of different sizes and supports robust exposure modeling. Table 1 clearly outlines the chosen indicators, developed through expert consultations and a review of relevant literature, their spatio-temporal resolution and concise definition. To ensure spatial consistency among datasets obtained at varying resolutions (as outlined in Table 1), all

Table 1
List of the indicators influencing HWR, along with their Spatio-temporal resolutions and data sources.

Risk Component	Indicator	Resolution		Data Source
		Spatial/ scale	Temporal	
Hazard	Temperature	≃2.2 km	Hourly	ERA5 downscaling (Copernicus Climate Change Service, 2023); COSMO—CLM model (https://doi.org/10.25424/cmcc/era5–2km_italy)
	Relative humidity	100 m	Hourly	Copernicus - Climate Change Service (C3S) (https://climate.copernicus.eu/)
	Wind speed	100 m	Hourly	Copernicus - Climate Change Service (C3S)
Exposure	Older population density	Census tract	Yearly	Municipality of Bologna (https://www.comune.bologna.it/)
Vulnerability (Sensitivity)	Gender	Census tract	Yearly	Municipality of Bologna
	Citizenship	Census tract	Yearly	Municipality of Bologna
	Social isolation	Census tract	Yearly	Municipality of Bologna
	LCZ	100 m	Static	WUDAPT (https://www.wudapt.org/)
	LULC	100 m	6-yearly	Copernicus Land Monitoring Service-CORINE (https://land.copernicus.eu/en/products/corine-land-cover)
Vulnerability (Adaptive Capacity)	EVI	30 m	16-day	Landsat 8 OLI/TIRS C2 Level 2 (https://doi.org/10.5066/P9OGBGM6)
	Proximity to green areas	Census tract	Static	Open Street Map (https://www.openstreetmap.org/)
	Distance to healthcare services	Census tract	Static	Open Street Map
	Distance to transportation	Census tract	Static	Open Street Map; Municipality of Bologna
	Distance to cool places	Census tract	Static	Open Street Map

environmental, socio-economic, and infrastructural data were harmonized to the census tract level, which served as the common spatial analysis unit. Raster datasets (e.g., temperature, vegetation indices) were aggregated using zonal statistics to calculate mean values per tract, while vector data (e.g., LCZs, health facilities) were spatially joined and summarized within tract boundaries. This preprocessing step ensured that all indicators contributing to hazard, exposure, and vulnerability were spatially aligned for integrated modeling and analysis.

Climatological data were obtained from Copernicus (Copernicus Climate Change Service, 2023), while demographic statistics were sourced from the Italian National Institute of Statistics-ISTAT: https://www.istat.it/en/. Socioeconomic data was derived from publicly available municipal records (Open Data Comune di Bologna). Most indicators, except for LULC, which is updated every six years, were developed at the census tract level in Bologna over a ten-year period (2014 to 2023). The proximity indicators are largely static over a decade. We utilized high-resolution ERA5-Land data, downscaled to ≃2.2 km using the COSMO CLimate Model (COSMO—CLM) (retrieved from https://doi.org/10.25424/cmcc/era5–2km_italy) to capture temperature dynamics, relative humidity and wind speed data at 10 m above ground (Raffa et al., 2021). Given the reliability of the downscaled temperature data over Bologna, we refer to the study by Raffa et al. (2021), which provides a comprehensive validation of the Very High Resolution Reanalysis for Italy (VHR-REA_IT) dataset. This dataset was generated using the COSMO—CLM model at a 2.2 km resolution and evaluated against ERA5 and the E-OBS observational dataset (~11 km resolution), covering the Bologna region. For the summer season (June–August), which is the focus of our study, the reported statistics for

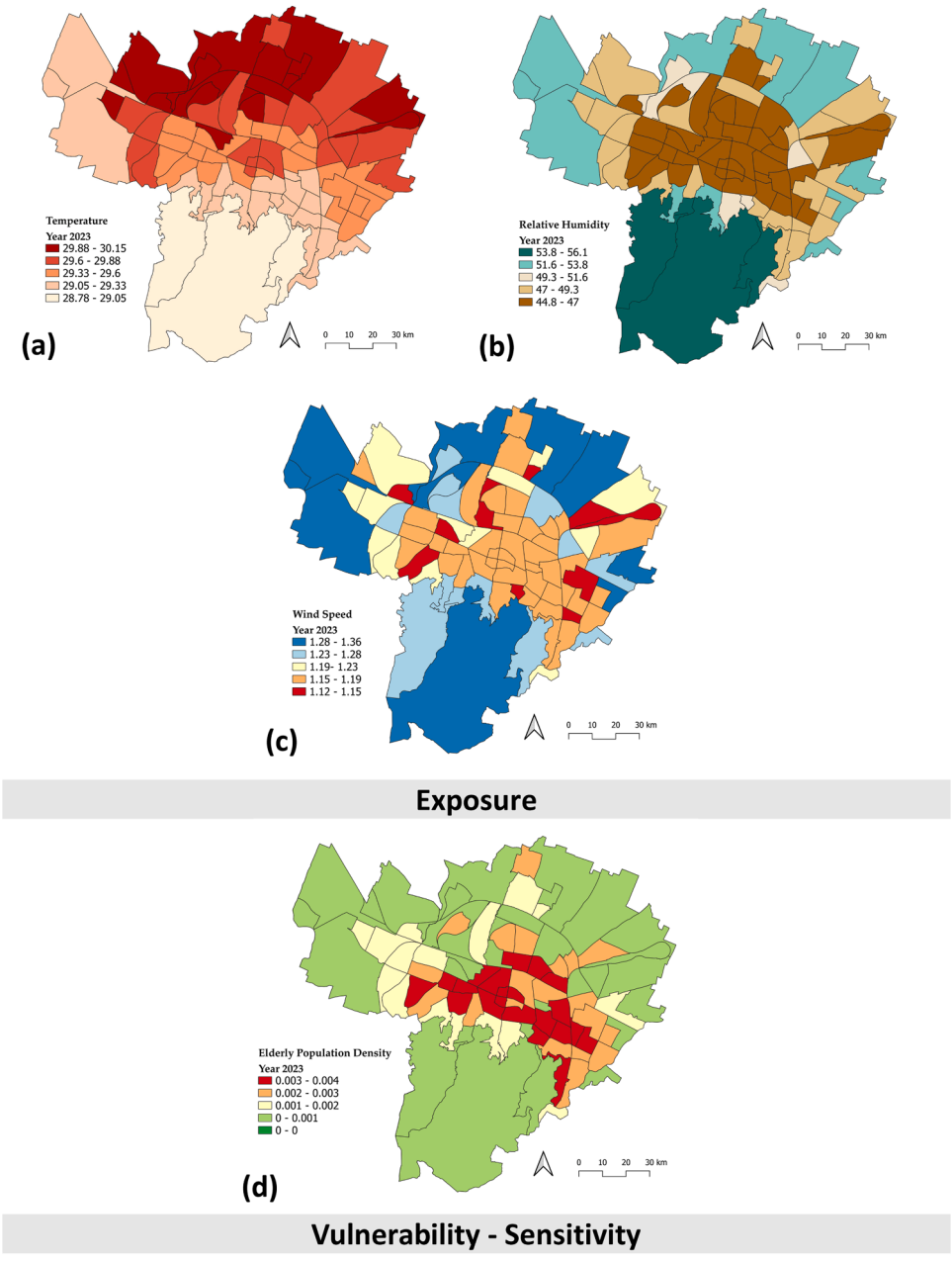

Fig. 4. Classification map of different indicators contributing to HWR across different districts of Bologna in 2023: a) Temperature, b) Relative humidity, c) Wind speed, d) Older population density, e) Gender (women), f) Citizenship (Foreign), g) Social isolation, h) LCZ, i) EVI, j) Proximity to green areas, k) Proximity to shelters, l) Proximity to public transportation, m) Proximity to cinemas, n) Proximity to healthcare services, o) Proximity to shopping centers, p) Proximity to public libraries, q) Proximity to all cool places.

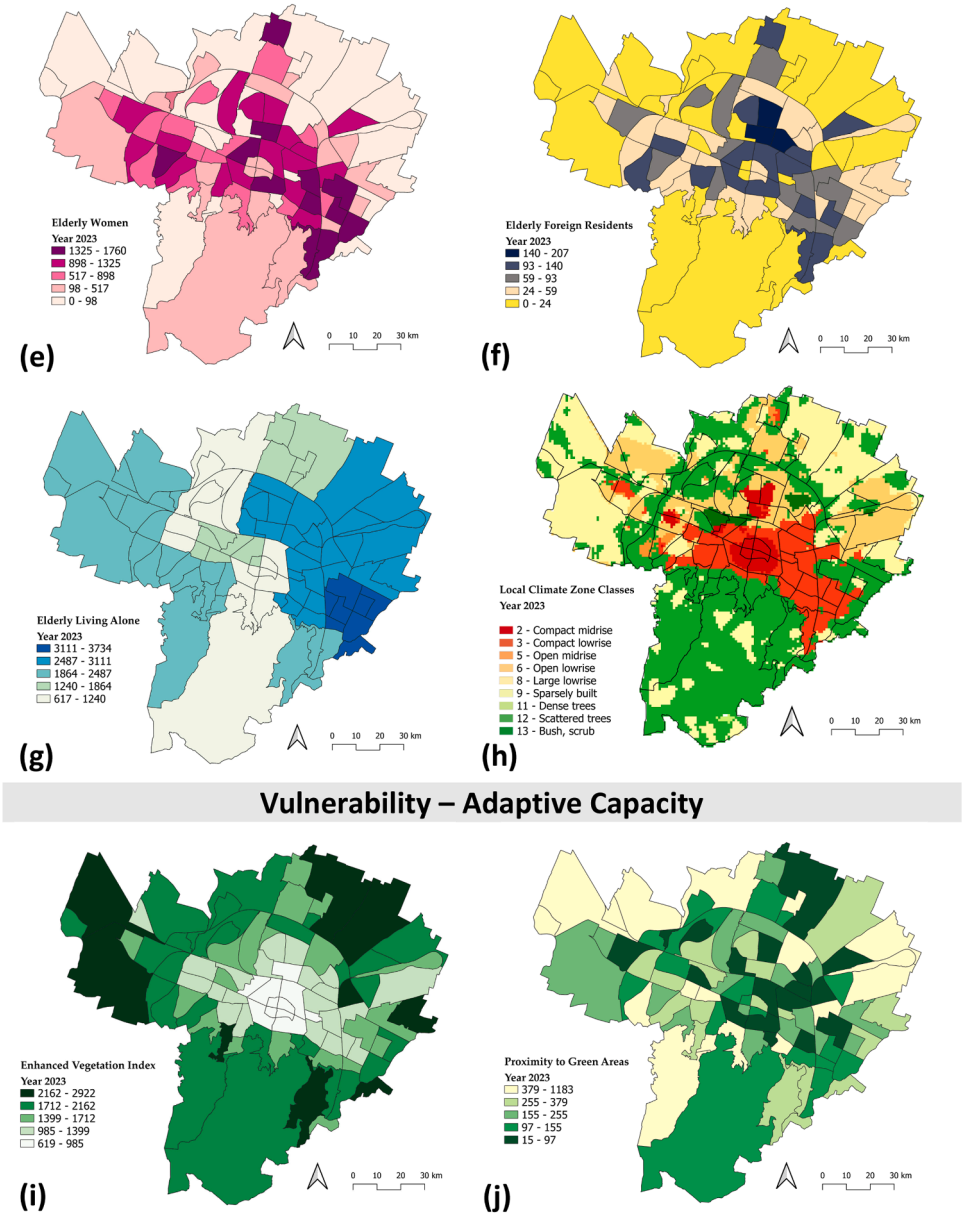

Fig. 4. (*continued*).

Northeast Italy (including Bologna) indicate a mean bias of +2.1 °C and a standard deviation ratio ($\sigma_{mod}/\sigma_{obs}$) of 1.3. Moreover, the study shows that COSMO—CLM outperforms ERA5 in reproducing extreme summer temperatures. These results confirm the suitability of the COSMO—CLM-based VHR-REA_IT dataset for climate analyses and impact assessments in Bologna, particularly during the summer season.

Land changes were analyzed using Corine Land Cover datasets for 2012 and 2018, which are provided by the Copernicus Land Monitoring Service and coordinated by the European Environment Agency. The urban layout was classified into 17 distinct LCZs using the World Urban Database and Access Portal Tools (WUDAPT) to facilitate microclimate studies. The EVI was derived by averaging Landsat 8 (OLI/TIRS C2 Level 2) images taken during the summer months (June–August), using only scenes with <8 % cloud cover. This approach ensures that vegetation health is assessed during the most heat wave-relevant season, while maintaining data quality by minimizing cloud contamination.

Demographic data from Bologna's Municipality web portal provided insights into the distribution of the older population, focusing on age, gender, and citizenship to assess vulnerability during heat waves. Data on older population residents living alone was used to identify communities at high risk of isolation (Kim et al., 2017). Older population density was analyzed as an exposure metric (Morabito et al., 2015), evaluating susceptibility to heat-related stress based on the density per square kilometer. Additional assessments focused on the distribution of green spaces (Gronlund et al., 2015), accessibility of healthcare facilities (Adams et al., 2022), proximity of public transportation (Karner, 2018), and availability of climate shelters such as public libraries, shopping malls, and cinemas to mitigate heat-related risks during heat waves (Bradford et al., 2015; Ellena et al., 2023). Spatial data for these amenities were sourced from OpenStreetMap (OSM) (https://www.openstreetmap.org/). Network analysis was used to calculate actual travel distances along roads and pathways, providing a practical evaluation of the accessibility of these climate shelters for residents. Fig. 4 illustrates the spatial distribution of the intensity of various parameters contribute to the HWR assessment across different districts of Bologna in 2023.

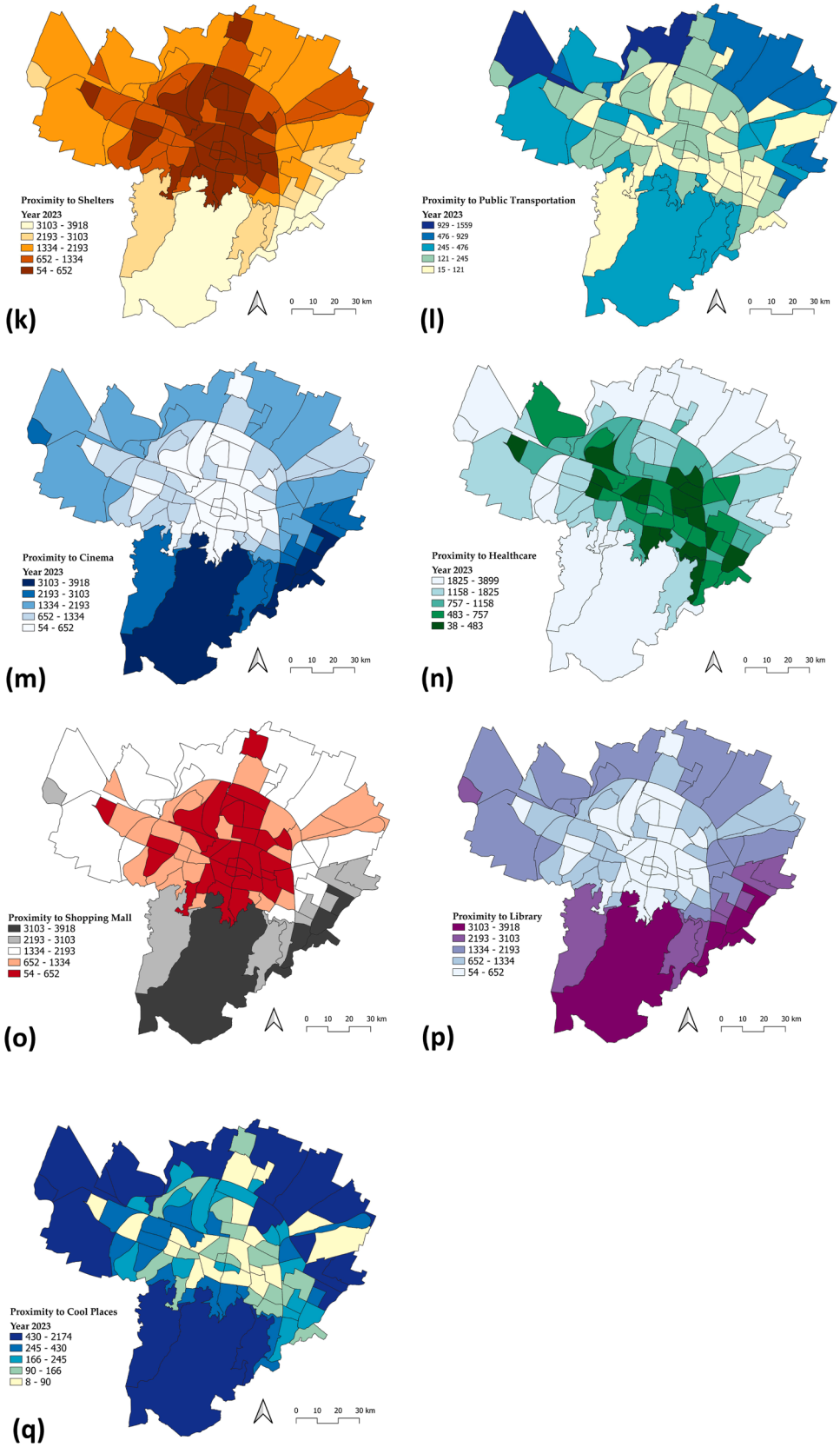

Fig. 4. (*continued*).

3.6. Reducing redundancy: multicollinearity and feature selection

To ensure model interpretability and accuracy, we assessed multicollinearity using both the correlation matrix and Variance Inflation Factor (VIF). The correlation matrix identifies strong linear relationships between variables (values near ± 1), while VIF quantifies the inflation of

variance due to correlated predictors. A VIF above 10 indicates high multicollinearity requiring adjustment, whereas values below 10 are acceptable (Hair et al., 2019). VIF was calculated using Eq. (4) as below.

$$VIF_j = \frac{1}{1 - R_j^2} \tag{4}$$

Where R_j^2 represents the coefficient of determination obtained by regressing the j-th predictor on all remaining predictors.

Feature selection is an essential phase in preprocessing ML models, particularly useful when managing large, high-dimensional datasets (Aksangür et al., 2022). This process not only boosts model performance by enhancing computational efficiency and interpretability but also helps in mitigating overfitting and reducing computational costs. In this study, we combined parametric and non-parametric statistical tests to refine feature selection. Parametric methods, like the ANOVA F-test, assume normally distributed data and identify features with strong linear relationships to the target variable (Jamil & Khanam, 2024). In contrast, non-parametric (distribution free) methods do not rely on distributional assumptions, making them more flexible for diverse datasets. We used Kruskal-Wallis test to identify key predictors in non-normally distributed data using rank-based comparisons (Hass & Ellis, 2019). By integrating these approaches, we selected only the most informative features, thereby improving both the accuracy and efficiency of our models. For detailed explanations of the ANOVA and Kruskal–Wallis methods, readers are referred to Fisher (1992) and Kruskal and Wallis (1952), respectively.

3.7. Data preparation: normalization and splitting

Effective data preparation is essential for building robust ML models. This includes data cleaning, format conversion, and scaling techniques such as normalization and standardization to ensure data quality and consistency. While standardization (e.g., z-score) is often preferred for its robustness to outliers (Pourzangbar et al., 2023a), in this study, the min-max normalization method (Eq. (5)) was used to scale all parameters between 0 and 1 to ensure comparability across features before input into the ML models.

$$X_N = \frac{X - X_{min}}{X_{max} - X_{min}} \tag{5}$$

where X_N is the normalized form of parameter X (scaled between 0 and 1); X_{max} *and* X_{min} represent the maximum and minimum value of the parameter X across the dataset, respectively.

Following normalization, the dataset was split into training and testing subsets to optimize model learning and generalization. Specifically, 70 % of the data was used for training the model, enabling it to learn patterns and relationships, while the remaining 30 % was reserved for testing to evaluate performance on unseen data (Côté et al., 2024). When needed, the training set was further partitioned into a validation subset for hyperparameter tuning and iterative refinement, helping to prevent overfitting and enhance model reliability on new data.

To develop the LSTM model, the dataset was reshaped into a three-dimensional structure with the format (samples, time steps, features). In this specific case, the samples correspond to 90 distinct regions, each identified by a unique GEOID. The time steps represent the years from 2014 to 2023, covering a 10-year period of interest. The features consist of 14 input parameters used to characterize each region over time. The target output is the HWR level assigned to each region, classified into five categories—'Very Low' (class 1), 'Low', 'Moderate', 'High', and 'Very High' (class 5)— using the Natural Breaks (Jenks) classification method (Jenks, 1963). This data-driven approach determines optimal breakpoints by minimizing within-class variance and maximizing variance between classes, ensuring that the resulting risk classes reflect meaningful distinctions in the spatial distribution of predicted risk values.

3.8. Long short-term memory

LSTM networks, introduced by Sepp and Jürgen (1997), are a specialized type of recurrent neural network, particularly well-suited for sequential data modeling due to its ability to capture both short- and long-term dependencies by retaining relevant past information through memory cells and gating mechanisms. Unlike traditional RNNs, LSTM incorporates a cell state and three gates including input, output, and forget gates that regulate the flow of information, enabling the model to learn from long sequences effectively. This architecture allows LSTMs to preserve context over extended periods, making them highly effective in capturing persistent extreme temperature patterns, which is critical for the early detection and forecasting of heat wave events (Qureshi et al., 2025). For a comprehensive overview of LSTM mechanisms and equations, readers are referred to Hochreiter and Sepp and Jürgen (1997) and Qureshi et al. (2025).

In this study, an LSTM neural network was employed to predict HWR in the city of Bologna, leveraging its proven capabilities for learning complex temporal patterns from climate time series. Specifically, the model incorporates 14 input features, as described in Section 3.5, including climatic variables (temperature, relative humidity, wind speed), environmental indicators (EVI, LCZ, LULC), and socio-demographic and spatial indicators such as elderly population density, elderly living alone, foreigner population, and distances to key urban amenities. Annual data were collected from 2014 to 2023, resulting in a 10-step temporal sequence for each spatial unit, which corresponds to census tracts or districts within the study area. This data structure aligns with the LSTM input format of (samples, time steps, features), resulting in a model input shape of (90, 10, 14)—with 90 spatial units, 10 annual time steps, and 14 features per time step. Among the features, temperature, humidity, wind speed, and EVI varied over time and contributed to the temporal learning capability of the model, while static or slowly varying features like LULC and population characteristics were held constant across time steps to provide contextual support. The LSTM model projected a value of HWR between 0 and 1 for each spatial unit. To make these outputs interpretable for decision-making, the projected continuous HWR values were classified into five distinct HWR levels—'Very Low', 'Low', 'Moderate', 'High', and 'Very High'— using the Natural Breaks (Jenks) classification method. This modeling approach allows the integration of both dynamic and static features in a spatio-temporal framework to effectively assess district-level HWR.

The model weights and biases during the training phase are determined using the Adam optimizer which aims to minimize the loss function Mean Squared Error (MSE). However, before training the model, the optimal hyperparameters are determined by the HOA (see section 2.8.1). To further ensure robustness against overfitting, early stopping monitors validation loss and ceases training if no improvement is observed after 100 epochs, enhancing model performance in practical applications. The Google Colab platform (https://colab.research.google.com/) was employed for model development and execution, using the Python programming language along with relevant algorithmic libraries.

3.8.1. Hippopotamus optimization algorithm

HOA, introduced by Amiri et al. (2024), is a nature-inspired optimization algorithm that mimics the behavior of hippopotamuses. It is a population-based method where each candidate solution is treated like a hippopotamus, representing a possible set of values to solve the problem. The algorithm is based on three main behaviors: young hippos exploring their surroundings, adult hippos defending their territory, and hippos escaping to water when in danger (Kudela & Matousek, 2022). Starting with random solutions, HOA updates each one step-by-step using rules that reflect these behaviors. This helps the algorithm explore a wide range of possibilities (exploration) and also focuses on improving the best solutions found so far (exploitation), leading to better and faster results. By mimicking these natural strategies, HOA

efficiently navigates complex, high-dimensional optimization landscapes, making it well-suited for fine-tuning ML models. In our case, this resulted in improved LSTM performance for time-series forecasting, demonstrating HOA's robustness, adaptability, and effectiveness in real-world optimization tasks.

The HOA relies on several key parameters that significantly influence its performance. These include the population size, the maximum number of iterations, the number of decision variables (dimensions), the lower and upper bounds for each variable, and the fitness function used to evaluate candidate solutions. In this study, the population size, representing the number of candidate solutions or "hippopotamuses" and typically ranges from 10 to 100 depending on the complexity of the optimization problem, was set to 50. The maximum number of iterations, which determines the total number of optimization steps and commonly varies between 50 and 500, was set to 500 in our implementation.

In this study, the HOA was employed to optimize key hyperparameters of the LSTM model. Each decision variable in the optimization process corresponds to a specific LSTM hyperparameter, including the number of LSTM units (neurons), number of hidden layers, learning rate, batch size, dropout rate, number of training epochs, and the activation function used in each layer. These parameters influence the model's learning capacity, convergence behavior, generalization ability, and temporal memory. The hyperparameter search space was defined as follows: number of LSTM units: {64, 128, 256}; dropout rate: {0.2, 0.3, 0.5}; learning rate: {0.0001, 0.001, 0.01}; batch size: {32, 64, 128}; number of epochs: {50, 100, 150}; activation functions: {tanh, ReLU, softmax, sigmoid}. The resulting optimization problem is 10-dimensional. The performance (fitness) of each candidate solution was evaluated using the Root Mean Squared Error (RMSE) between the LSTM-projected values and the observed HWR values.

3.9. Validation methods

Model validation is a crucial step in assessing the accuracy and robustness of ML models, employing a range of metrics and methods to ensure reliability and precision. This process typically involves reserved data to test the model using statistical metrics such as Correlation Coefficient (CC), RMSE, Mean Absolute Error (MAE), as well as classification-specific measures like Accuracy, Precision, Recall, and F1-score.

For the assessment of our model's performance, we employed a confusion matrix, an essential tool that provides a tabular visualization of the model's predictions against actual labels. This matrix facilitated the calculation of Precision, Recall, and F1-score, key metrics that respectively assess the Accuracy of positive predictions, the model's ability to identify all relevant instances, and a weighted average of Precision and Recall. Additionally, we conducted Sensitivity Analysis (SA) to understand how variations in input parameters affect the model's output. Utilizing the Average Percentage Change (APC) method (Pourzangbar et al., 2017b), this analysis helped pinpoint the most influential parameters, guiding precise calibration to enhance model accuracy and stability.

Accuracy measures the proportion of all correct predictions (both true positives and true negatives) out of the total number of predictions. It is useful when classes are balanced. However, it can be misleading in imbalanced datasets, where a high accuracy may be achieved by always predicting the majority class (Eq. (6)).

$$\text{Accuracy} = \frac{TP + TN}{TP + TN + FP + FN} \tag{6}$$

Where TP is True Positives, TN is True Negatives, FP is False Positives, and FN is False Negatives.

Precision, known as positive predictive value, measures the proportion of positive predictions that are actually correct. A model with high precision makes fewer false results (Eq. (7)).

$$\text{Precision} = \frac{TP}{TP + FP} \tag{7}$$

Recall measures the ability of the model to correctly identify all relevant positive cases in the dataset. It is important when the cost of missing a positive case is high (e.g., medical diagnoses). A high recall means fewer false negatives (Eq. (8)).

$$\text{Recall} = \frac{TP}{TP + FN} \tag{8}$$

F1-score is the harmonic means of precision and recall, offering a balanced measure that penalizes extreme values of either metric. F1-score is particularly useful in imbalanced datasets where both false positives and false negatives are significant. It provides a single metric to balance the trade-off between precision and recall (Eq. (9)).

$$F1 - \text{score} = \frac{2 \times \text{Precision} \times \text{Recall}}{\text{Precision} + \text{Recall}} \tag{9}$$

The APC is used to quantify the average rate of change of a variable over a specific period, expressed as a percentage. It is particularly useful for analyzing trends in time-series data, such as temperature anomalies and health outcomes (Eq. (10)).

$$\text{APC} = \frac{1}{n} \sum_{i=1}^{n} \left(\frac{X_i - X_{i-1}}{X_{i-1}} \right) \times 100 \tag{10}$$

Where X_i is the value of the variable at time step i, X_{i-1} is the value at the previous time step, and n is the total number of changes (i.e., time intervals).

3.10. Model explainability

ML models, often described as "black boxes," lack inherent explainability and interpretability, raising concerns in critical applications like predicting heat waves. Explainability involves understanding the model's reasoning for specific predictions, while interpretability relates to comprehending the implications of these predictions based on the input data (Aydin & Iban, 2023).

In this study, we employed the PDP technique to interpret the behavior of the machine learning model used to predict heat wave-related risks. PDPs serve as a powerful model-agnostic tool for explaining how individual features (or feature pairs) influence the predicted output, even when the model itself is a complex black box (Gunes, 2023). A PDP visualizes the marginal effect of one or two selected features on the model output by averaging over the values of all other features in the dataset. Mathematically, the PDP function for a subset of features reads as Eq. (11) (Su et al., 2021):

$$\widehat{f}_S(x_S) = E_{X_C}[\widehat{f}(x_S, X_C)] = \int \widehat{f}(x_S, X_C)\, dP(X_C) \tag{11}$$

Where E_{X_C} represents the expected value with respect to the distribution of the complementary features X_C, $dP(X_C)$ is the probability measure over the distribution of X_C, x_S are the features of interest (subset S), and X_C are the remaining features not in S, treated as random variables.

The function $\widehat{f}$ is the trained machine learning model. The goal of PDP is to compute the marginal effect of features in x_S on the model output by integrating out the influence of all other features in X_C.

In this work, we applied one-way PDPs, each analyzing a single feature at a time, on the most influential environmental, climatic, and demographic predictors. These plots were particularly effective in revealing nonlinear dependencies, inflection points, and critical thresholds associated with heightened HWR. To aid interpretation, we highlighted the region around the maximum PDP value for each feature, as these represent the intervals where the model response is most sensitive to change. Importantly, the PDP values were averaged across all

five output classes of our multi-class classification model, providing a global view of feature effects across the entire risk spectrum.

3.11. Model deployment

Our study reaches a pivotal stage during the deployment phase, transitioning from theoretical models to practical applications. By implementing the LSTM model, we assessed the HWR under various future climate scenarios indicated by RCPs. These scenarios project diverse future climates influenced by differing levels of greenhouse gas emissions, pivotal for anticipating changes in climatic variables such as temperature. We focused on RCPs 4.5, 6.0, and 8.5, each reflecting a unique scenario of climate change impact. Each scenario underlines the necessity for tailored adaptation strategies for urban centers like Bologna by 2050, focusing on temperature variations and evaluating the robustness of green infrastructure using EVI and proximity to the urban green areas to gauge their effectiveness in mitigating HWR. The significance of green infrastructure in urban heat mitigation is increasingly critical (Wong et al., 2021). Our use of EVI to assess the health and robustness of urban vegetation underscores its role in enhancing urban cooling through processes such as evapotranspiration and solar radiation reflection, providing a natural counter to rising temperatures. The health benefits of urban green spaces have been found to depend on their availability, accessibility, visibility, and specific characteristics (Labib et al., 2020). Proximity to green spaces (Pinto et al., 2022), particularly within 100 to 300 m, has been associated with increased physical activity, with effectiveness declining beyond 400 m (or 10 min walking) (Ayala-Azcárraga et al., 2019).

Our study leveraged EVI to precisely measure these effects, aiding urban planners in developing strategies to fortify city resilience against anticipated climate change impacts. Meanwhile, examining the interaction between temperature fluctuations, the health of green spaces, and proximity to greenery, our model assists in planning effective and targeted urban adaptations. The strategic application of these nature-based solutions help urban planners identify areas for potential green enhancements, such as tree plantings and the development of green roofs as climate shelters, particularly in areas with limited canopy coverage and high HWRs.

4. Results and discussion

4.1. Multicollinearity analysis

Various parameters such as temperature, relative humidity, wind speed, older population density, LULC, LCZ, EVI, and distances to essential services contribute to HWR. Insights from the correlation matrix (Fig. 5) revealed intricate relationships between these factors: temperature and relative humidity displayed a slight negative correlation (−0.13), suggesting that higher temperatures typically lead to lower humidity levels. Older population densities showed a strong negative correlation (−0.65) with LULC, indicating that areas with more older population residents may lack beneficial land cover (i.e., vegetated and water-rich surfaces such as urban parks, green roofs, and water bodies that help mitigate heat through evapotranspiration and shading, contrasting with impervious surfaces that intensify heat stress (Bowler et al., 2010)), increasing their vulnerability to heat waves. Conversely, a strong positive correlation (0.66) between relative humidity and EVI highlighted vegetation's role in sustaining moisture levels, mitigating some heat wave effects. There was a very high positive correlation (0.82) between the older population female population and older population density, pointing to the significant presence of older population women in densely populated older population areas. Moderate positive correlations were observed between the distance to cooling places and the distance to greenery (0.47), and between the distance to public transportation and cooling places (0.57), showing that areas farther from cooling resources also tended to lack green spaces and adequate transportation, compounding their risk during heat waves.

The correlation matrix reveals that most input parameters exhibit weak to moderate linear relationships with heat wave severity (represented by temperature), with no single parameter showing a dominant influence. Some variables, such as wind speed, distance to cooling centers, and distance to healthcare, display negligible correlations with temperature. However, these variables may still capture important nonlinear or indirect effects, particularly when considering vulnerability and exposure aspects. Therefore, all parameters will be retained for further analysis to ensure a comprehensive representation of factors contributing to heat wave severity.

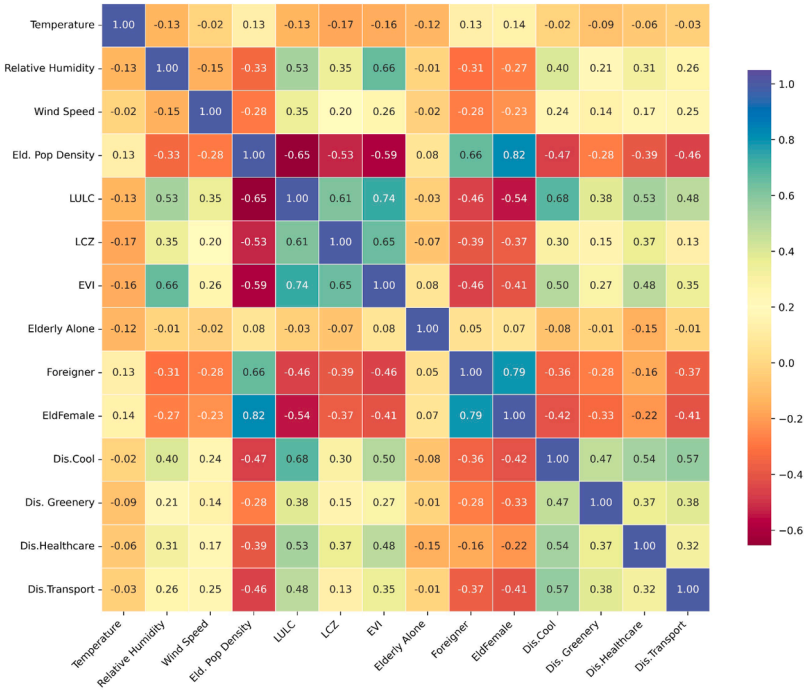

Fig. 5. Heatmap of correlation coefficients between various parameters contributing to HWR assessment.

An inspection of the VIF analysis (Table 2) reveals that all parameters have VIF values below the critical threshold of 10, confirming manageable levels of collinearity and justifying their inclusion in the model. Temperature exhibits minimal collinearity with a very low VIF of 1.34. Wind speed and LCZ show moderate multicollinearity with VIFs of 7.37 and 5.83, respectively, and the distance to greenery registers a VIF of 3.22. Despite nearing the upper limit with VIFs around 10, parameters such as older population density, older population living alone, and LULC are retained due to their significant roles in enhancing the understanding of heat wave impacts.

4.2. Feature selection

Inspection of the ANOVA results reveals that distance to public transportation is the most significant factor, contributing 14.56 % to overall importance and emphasizing its critical role in emergency management during heat waves. EVI and LCZ follow with 13.54 % and 12.36 %, respectively, highlighting their influence in reducing heat wave severity. Wind speed and proximity to green spaces are also significant, with contributions of 12.27 % and 11.39 %, respectively, due to their roles in promoting heat dispersion and enhancing cooling effects that mitigate the UHI effect. Access to healthcare is notably important at 11.47 %, underscoring its relevance during heat wave emergencies. Relative humidity (6.76 %), demographic factors such as the older population living alone (5.73 %) and non-Italian citizenship (3.05 %) indicate specific vulnerabilities. In contrast, older population density (3.17 %), proximity to cool places (4.15 %), LULC (0.02 %), and older female population (0.30 %) exhibit minimal impact.

The Kruskal–Wallis results highlight temperature as the most influential factor, contributing 19.5 % to the overall importance. LCZ also shows significant impact at 16.5 %, reflecting its role in heat distribution. Proximity to greenery is notable at 14.3 % due to its cooling effects. Wind speed and EVI contribute to climate modification and urban cooling, with respective importances of 14.05 % and 9.74 %. Lesser impacts are observed from relative humidity (6.50 %), access to healthcare (6.00 %), and the older population living alone (5.10 %). Factors such as foreign nationalities (2.48 %), proximity to cool places (2.16 %), older population density (1.55 %), LULC (0.83 %), older female population (0.81 %), and distance to public transportation (0.38 %) exhibit minimal influence Fig. 6.

4.3. Model configuration and hyperparameters

To fine-tune the hyperparameters of the LSTM model, we employed the HOA, which systematically explores the hyperparameter space to identify the most effective configuration. The sequential processing begins with the first LSTM layer, comprising 128 units and using a tanh activation function. The "return sequences" parameter is enabled to ensure that the output is passed to subsequent layers. This is followed by a dropout layer with a rate of 0.3, which helps prevent overfitting by randomly omitting 30 % of the units during training. A second LSTM layer, similar in structure, maintains sequence continuity, followed by a batch normalization layer that stabilizes and accelerates training while improving generalization. A time-distributed dense layer is then used to make timestep-specific predictions, applying a SoftMax activation function suitable for multi-class classification tasks.

The initial hyperparameter search space includes the number of LSTM units (64, 128, 256), dropout rates (0.2, 0.3, 0.5), learning rates (0.001, 0.01, 0.0001), batch sizes (32, 64, 128), number of epochs (50, 100, 150), and activation functions (tanh, ReLU, SoftMax, and Sigmoid). These parameters are optimized using HOA to determine the best-performing configuration, as detailed in Table 3.

Table 2
VIF values for different spatial input parameters.

Parameter	VIF	Remark
Temperature	1.34	Conserved
Relative Humidity	9.28	Conserved
Wind Speed	7.37	Conserved
Older population Pop Density	10.08	Conserved
LULC	9.37	Conserved
LCZ	5.83	Conserved
EVI	8.88	Conserved
Older population Alone	9.33	Conserved
Foreigner	5.46	Conserved
Older population Female	9.08	Conserved
Distance to Cool Places	4.35	Conserved
Distance to Greenery	3.22	Conserved
Distance to Healthcare	5.36	Conserved
Distance to Transportation	3.43	Conserved

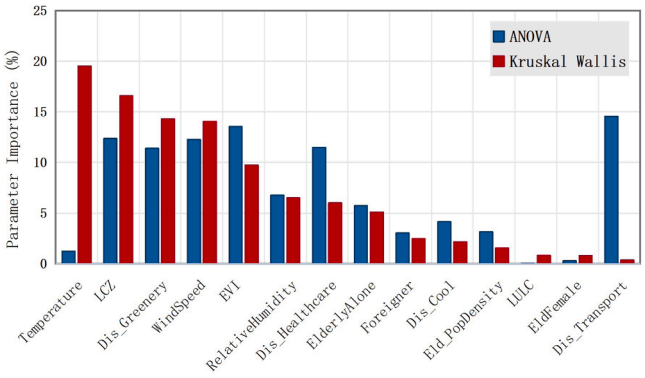

Fig. 6. Results of ANOVA and Kruskal Wallis utilized for the feature selection of susceptibility of HWR.

4.4. Model performance

4.4.1. Confusion matrix

The confusion matrix presented in Fig. 7 evaluates the LSTM model's performance in predicting HWR categories: 'Very Low', 'Low', 'Moderate', 'High', and 'Very High'. The model demonstrates strong accuracy in the 'Very Low' category with a correct classification rate of 77.76 %. However, some misclassifications occur in the 'Low', 'Moderate', and 'Very High' categories, with rates of 5.12 %, 4.72 %, and 6.89 %, respectively. For the 'Low' category, the model achieves 73.80 % accuracy, though it occasionally confuses this class with 'Very Low' and 'Moderate' categories. The 'Moderate' category shows a lower accuracy of 65.31 %, with significant misclassifications into 'Very Low' and 'Very High' categories, indicating greater uncertainty in middle-range risk levels. In contrast, the model performs well in the 'High' category, attaining an accuracy of 78.72 % with minimal classification errors. The

Table 3
Optimal hyperparameters of the developed LSTM model identified via the HOA algorithm.

Hyperparameter	Description	Range
Number of layers	Stacked LSTM depth	2
Number of Units	Number of units in each LSTM layer	[128, 64]
Dropout Rate	Fraction of units to drop for regularization	0.3
Learning Rate	Step size during optimization	0.01
Batch Size	Size of data chunks per gradient update	64
Number of Epochs	Total iterations over the training data	100
Sequence window length	Timesteps	10
Activation function in LSTM layers	Input, Forget, Output Gates	Sigmoid
	Cell State (candidate values)	Tanh
	Final Output Layer	SoftMax

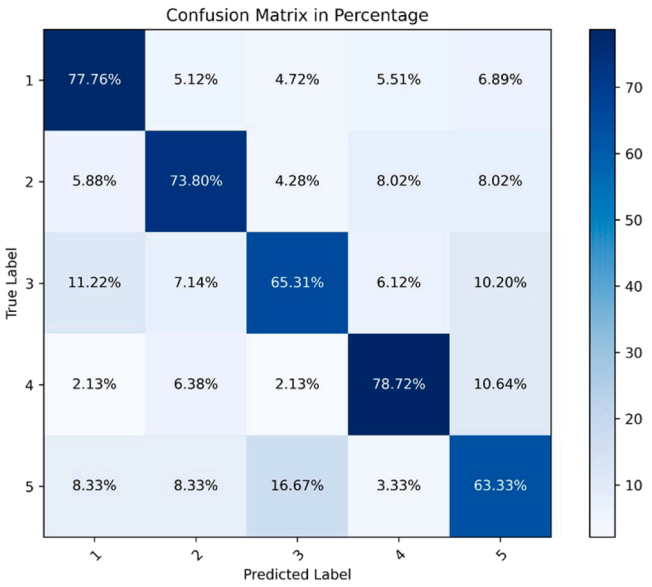

Fig. 7. Confusion matrix of predicted HWR classes utilizing the LSTM model.

'Very High' category has the lowest accuracy at 63.33 %, with notable misclassifications particularly into the 'Moderate' and 'Low' categories. Overall, the model exhibits robust predictive performance, especially for the 'Very Low', 'Low', and 'High' categories, each achieving over 70 % classification accuracy.

The comparison chart between predicted and observed classes of heatwave-associated risk (Fig. 8) illustrates the model's performance across different severity levels. The model shows a close alignment with observed values in the 'Low' and 'Moderate' categories, predicting proportions of 0.199 and 0.119, respectively, compared to observed rates of 0.208 and 0.109. This indicates effective calibration for intermediate risk levels. However, the model underestimates the 'Very Low' category, with a predicted rate of 0.470 versus an observed value of 0.564. This suggests a conservative bias that reduces the likelihood of overpredicting low-risk cases. In contrast, the model slightly overestimates the 'High' and 'Very High' categories, predicting 0.098 and 0.114, respectively, against observed values of 0.052 and 0.067. This tendency reflects the model's heightened sensitivity to higher-risk scenarios, which may be beneficial for precautionary public health measures.

To better understand the model's predictive performance, we examined both the confusion matrix and the distribution of predicted versus observed classes. Two key factors contribute to the observed misclassifications. First, most errors occur between adjacent risk levels, particularly between 'Medium' and 'High' or 'Medium' and 'Low' categories. This is likely due to overlapping environmental and demographic features in transitional zones, where small variations in parameters such as vegetation cover, green space accessibility, or

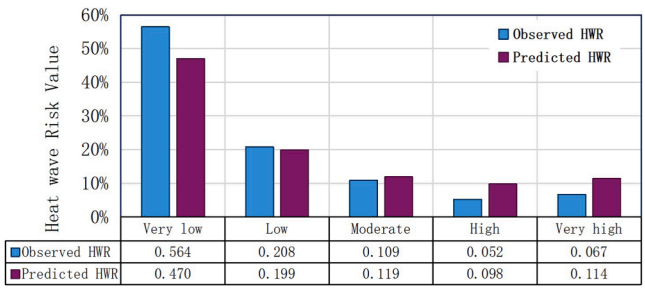

Fig. 8. Comparison of observed and predicted HWR percentages across different risk levels.

population composition can lead to class ambiguity near decision boundaries. Second, as illustrated in Fig. 8, the distribution of observed samples is highly imbalanced, with the majority concentrated in the 'Very Low' risk class and far fewer in the 'Very High' category. This imbalance may have biased the model during training, resulting in underprediction of the dominant class and overprediction of minority ones. Together, these factors highlight the complexity of modeling HWR and suggest that future work should consider techniques such as resampling or class-weighted optimization to improve classification robustness across all risk levels.

4.4.2. Performance metrics

The performance of the developed LSTM model in classifying HWR into five distinct categories is evaluated using key metrics: Accuracy, Precision, Recall, and F1-score. To preserve the temporal integrity of the time series data, the model is trained and validated using K-fold cross-validation with the TimeSeriesSplit technique, an approach based on walk-forward validation. This method maintains the chronological order within each fold and prevents information leakage by avoiding random shuffling, which is essential for sequential models like LSTM. Table 4 reports the average values of the evaluation metrics across all folds ($K = 10$), while Fig. 9 presents violin plots to visualize their distribution during cross-validation. The results indicate that the LSTM model performs best in predicting the 'Very Low' risk class, with an Accuracy of 0.93, Precision of 0.78, Recall of 0.85, and an F1-score of 0.75, demonstrating high reliability. For the 'Low' class, the model maintains consistent performance (Accuracy: 0.77; Precision: 0.74; Recall: 0.75; F1-score: 0.75). In the 'Moderate' class, the model achieves moderate reliability with Accuracy at 0.60, Precision at 0.65, Recall at 0.62, and an F1-score of 0.75. While the 'High' risk class shows a lower Accuracy of 0.42, it achieves a high Recall of 0.79, indicating strong sensitivity in detecting higher-risk cases despite limited Precision. Lastly, the 'Very High' category exhibits an Accuracy of 0.67, Precision of 0.63, Recall of 0.57, and an F1-score of 0.75, suggesting some limitations in differentiating the most severe cases, though the model remains moderately effective overall.

4.5. Generated heat wave risk maps

The heat wave hazard index, utilizing the 95th percentile of summer temperatures from the past decade, was utilized to measure the intensity, frequency, and duration of heat waves. Heat wave events were defined as temperatures exceeding this threshold for at least three consecutive days. Building on this, an exposure map was developed to identify areas where populations and physical assets are most at risk due to varying levels of exposure. Additionally, a vulnerability map was constructed using socio-economic and demographic indicators to reflect the capacity of different communities to cope with and respond to heat wave impacts. For the sake of simplicity, this section focuses solely on the spatial distribution of HWR components for the year 2023. Fig. 10 presents the individual components such as hazard, exposure, and vulnerability derived from observed and collected data, which were integrated into a comprehensive risk model utilizing the risk formula

Table 4
The performance of the developed LSTM model in calculating the HWR across different risk levels in terms of statistical indices.

Class	Statistical Index			
	Accuracy	Precision	Recall	F1-score
Very low	0.93	0.78	0.85	0.75
Low	0.77	0.74	0.75	0.75
Moderate	0.60	0.65	0.62	0.75
High	0.42	0.79	0.55	0.75
Very high	0.67	0.63	0.57	0.75
Full data	0.67	0.72	0.66	0.75

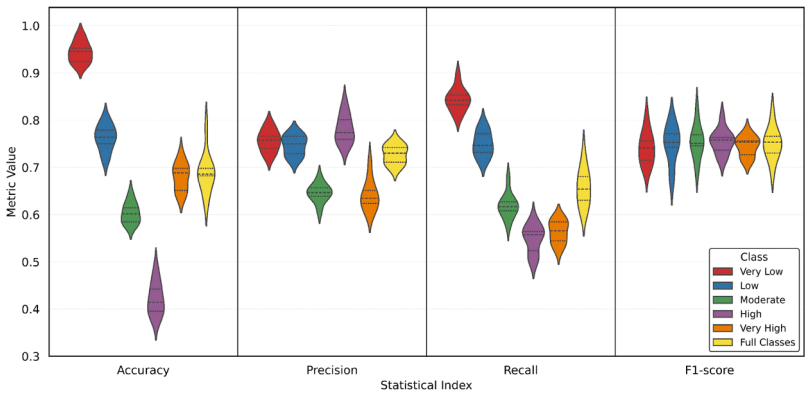

Fig. 9. The Violin plot represents the developed LSTM model's performance in calculating the HWR across different risk levels considering K-fold cross validation technique with $K = 10$.

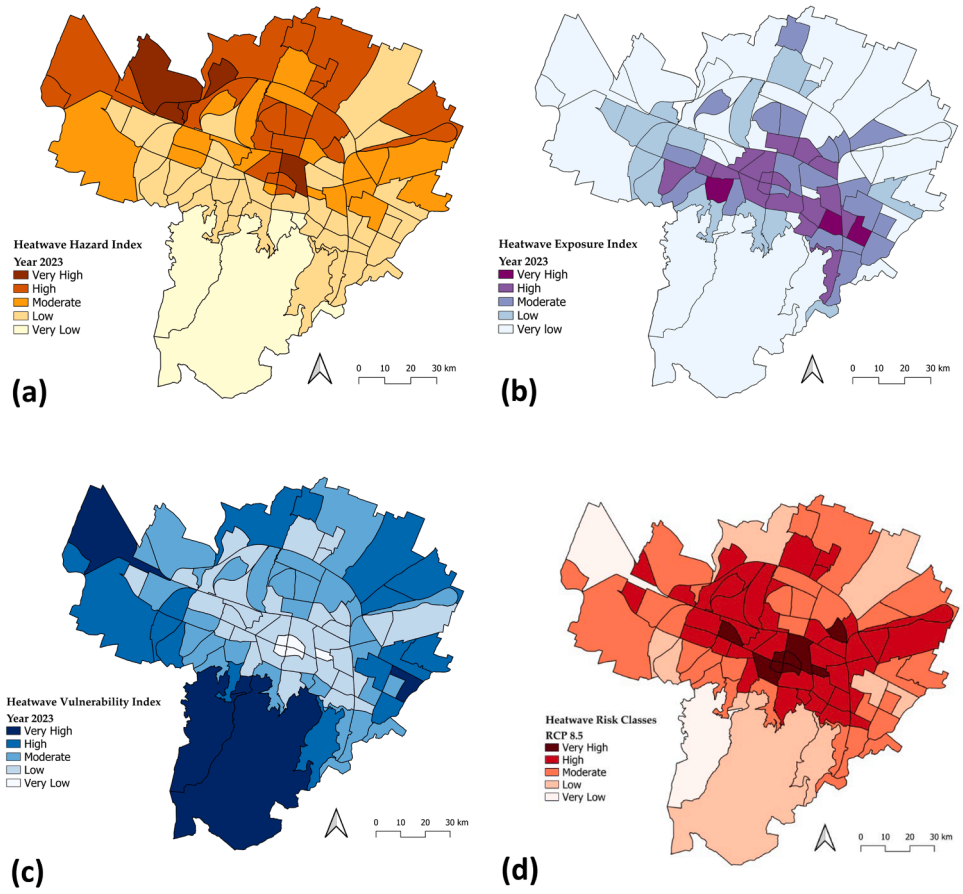

Fig. 10. Observational spatial patterns of HWR components in 2023: (a) Hazard, (b) Exposure, (c) Vulnerability, and (d) Overall Risk Index; Classified into five levels: Very Low, Low, Moderate, High, and Very High.

Risk $=$ Hazard $\times$ Exposure $\times$ *Vulnerability*.

The spatial patterns in the observed and predicted HWR maps for Bologna in 2023 exhibit a high degree of concordance, particularly across the central, western, and southern districts of the city. The model effectively identifies zones characterized by 'Very High' and 'High' HWR, demonstrating strong agreement with observed heat-related data. This consistency is further reinforced by the difference map (Fig. 11), in which the majority of spatial units are labeled as True, indicating correct classification.

Fig. 12 highlights the differences between observed and LSTM-predicted HWR classes. Areas marked in green indicate correct predictions where the observed and predicted classes correspond, while areas in orange represent classification discrepancies. These deviations are spatially constrained and affect only a minority of zones, typically occurring along the boundaries between adjacent risk levels, such as 'Moderate' vs. 'High' or 'Low' vs. 'Moderate'. This suggests that the classification errors are primarily marginal and do not substantially affect the overall trend direction or spatial distribution patterns. Consequently, while misclassifications are present, they are not severe enough to compromise the model's predictive value—particularly since most errors fall within one risk level rather than between extremes (e.g., 'Very Low' erroneously classified as 'Very High').

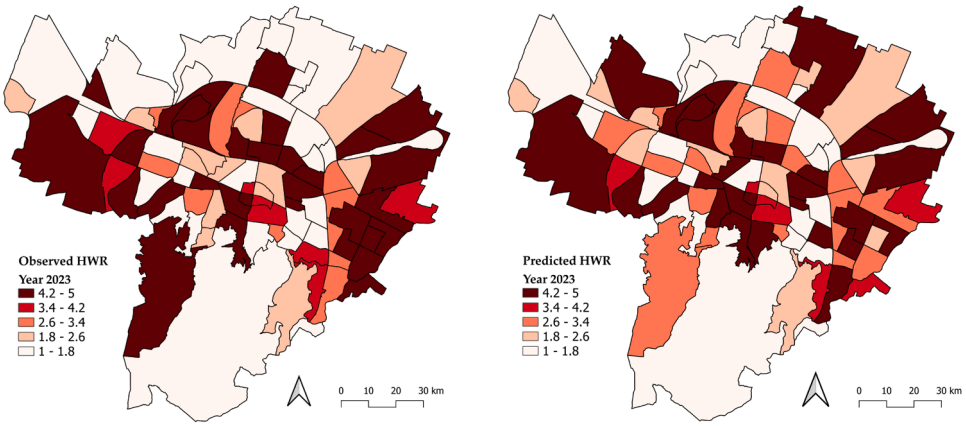

Fig. 11. The spatial distribution maps of HWR classes in Bologna in 2023; Observed (left) and predicted by the developed LSTM model (right).

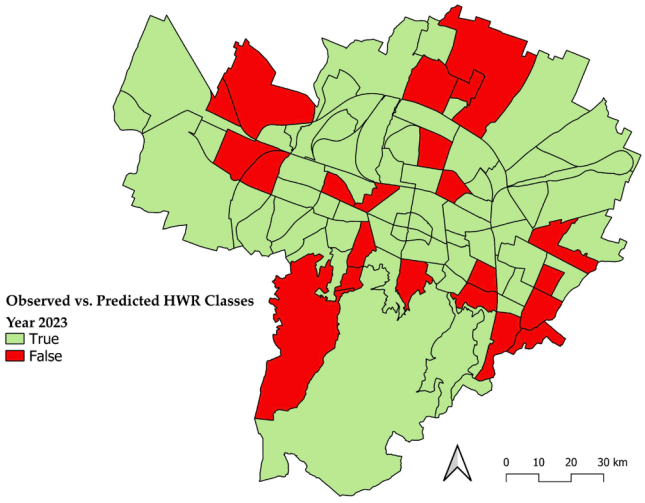

Fig. 12. Difference of observed and predicted maps of HWR classes (Year 2023).

4.6. Partial dependence plots

To examine the influence of individual features on HWR levels, we applied the PDP technique, averaged across all classes, to selected input variables. This approach isolates the effect of a single feature on the predicted outcome by averaging out the influence of all other variables. A higher PDP value indicates that the model tends to predict a higher HWR for the corresponding feature value. The PDPs reveal critical associations between temperature, relative humidity, and HWR. Specifically, temperatures exceeding 29 °C and relative humidity above 48 % correspond to increased PDP values, indicating elevated HWR under these conditions (Sobolewski et al., 2021). This aligns with established meteorological thresholds for heat-related health impacts. On humid days, apparent temperature increases due to reduced evaporative cooling via sweating. Since sweating is the body's primary thermoregulation mechanism (Baker, 2019), high humidity impairs this process, increasing the risk of heat exhaustion, heat stroke, and related illnesses, particularly among older populations (Sobolewski et al., 2021).

The co-occurrence of extreme heat and high humidity, as during the 1995 Chicago heat wave, has been linked to severe health impacts and excess mortality (Sarofim et al., 2016). Recent studies report that in regions such as the Midwestern and Eastern U.S., China, and Northern Latin America, humidity intensifies the severity of heat waves. Projections suggest that under a 4 °C warming scenario, apparent temperatures exceeding 55 °C may occur biennially in some regions, surpassing physiological tolerance limits and underscoring the urgent need for adaptation and mitigation (Russo et al., 2017).

HWR is also elevated in areas with low wind speeds (below 1.1 m/s), likely due to diminished convective cooling. Urban morphology indicators such as LULC and LCZ show clear peaks in PDP values, with built-up and densely urbanized areas associated with higher HWR, consistent with the UHI effect. Demographic features, including the density of older female populations and the proportion of foreign nationals, exhibit distinct thresholds at which vulnerability increases. For instance, HWR peaks where the older population density approaches 0.001, reflecting elevated risk due to factors like social isolation and reduced mobility. Environmental indices such as EVI also demonstrate non-linear effects. Regions with low EVI values (below 1000), indicative of sparse vegetation, are linked to higher HWR. In contrast, HWR declines significantly as EVI exceeds 2000, likely reflecting the cooling influence of vegetation and associated land surface characteristics. Accessibility-related variables including distances to healthcare facilities and public transportation show rising PDP values at greater distances (e.g., >3000 m and >1250 m), suggesting heightened vulnerability in less accessible regions. The highlighted intervals in each subplot of Fig. 13, centered around the peak PDP values, mark the most critical ranges and provide actionable insights for spatially targeted resilience planning and infrastructure upgrades.

4.7. Risk mapping under representative concentration pathways

In this study, future climate projections were based on three RCPs (RCP 4.5, RCP 6.0, and RCP 8.5) obtained from the EURO—CORDEX regional climate modeling initiative. Specifically, we used downscaled outputs from the COSMO—CLM regional climate model, which provides simulations of future climate conditions at a spatial resolution of ≃2.2 km. These datasets were not derived from reanalysis products such as ERA5, but rather from global climate models (GCMs) downscaled using dynamical methods to produce high-resolution future scenarios. From these RCP datasets, we extracted a key climate variable including maximum and minimum temperature for the summer months (June, July, August) from 2014 to 2023. These temporally-averaged parameters were used as inputs to our LSTM-based HWR modeling framework.

The findings reveal a substantial shift from lower risk categories ('Very Low' and 'Low') to higher ones ('High' and 'Very High'), indicating a rise in areas vulnerable to severe heat waves as greenhouse gas emissions intensify. Under the worst-case scenario, RCP 8.5, areas classified as 'Very Low' risk are projected to decline from 30 % in 2023 to 13 % by 2050, while those in the 'Very High' risk category may nearly double from 34 % to 66 %. Even under the milder RCP 4.5, 'Very High' risk areas are expected to increase to 51 %, underscoring a notable intensification of heat wave conditions. Interestingly, the 'Moderate'

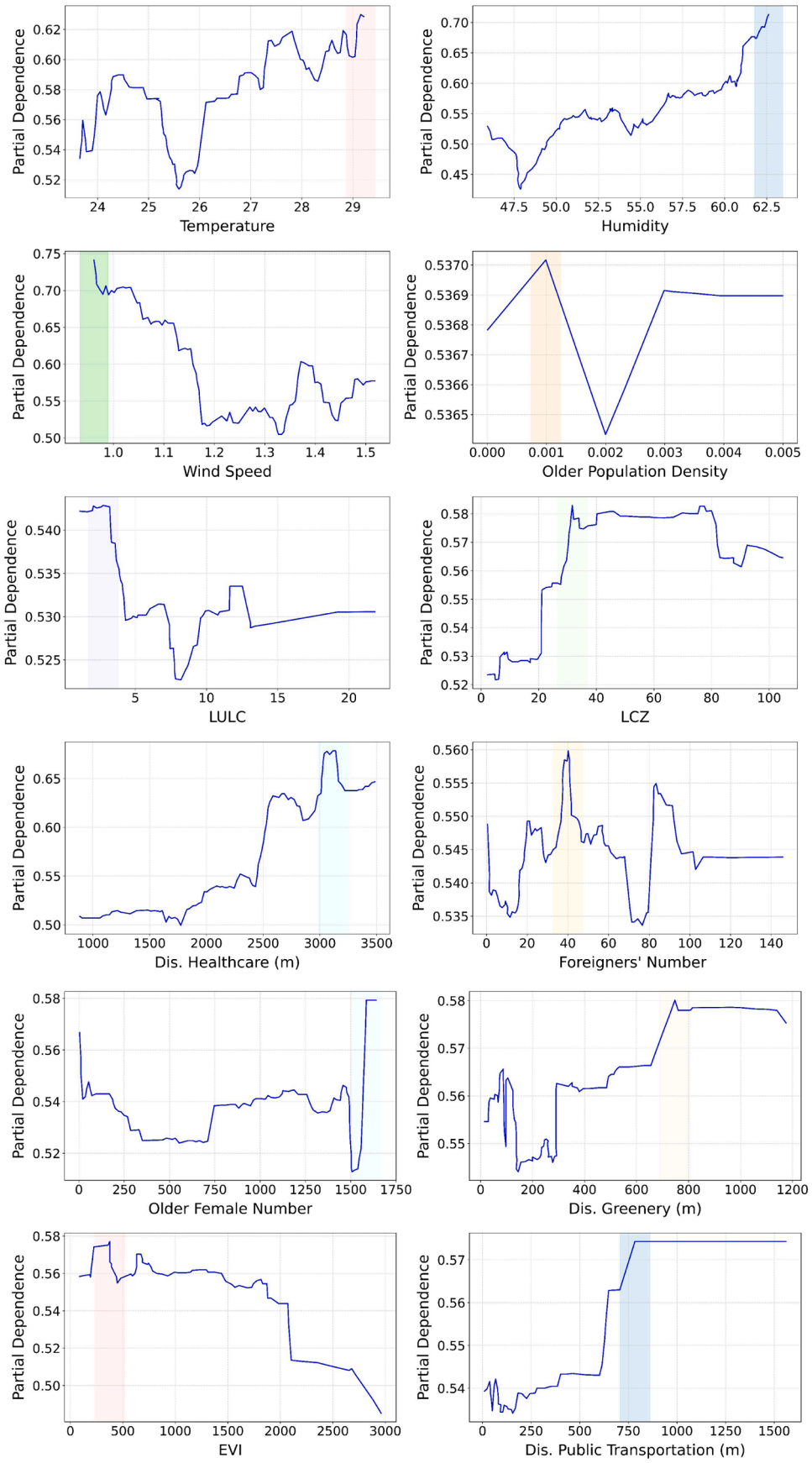

Fig. 13. PDPs for interpreting the influence of selected environmental, climatic, and demographic factors on HWR. Highlighted regions represent the intervals of each variable with the strongest impact on HWR and PDP values which are averaged across all classes.

category shrinks under RCP 8.5, reflecting a redistribution toward more extreme risk levels. Meanwhile, the 'High' category shows variability, rising slightly under RCP 6.0 and then declining to 5 % under RCP 8.5. These dynamics, detailed in Table 5 and illustrated in Fig. 14, highlight the escalating threat posed by heat waves and reinforce the urgency of mitigation strategies. This progression is critical for preparing urban centers like Bologna to confront more frequent and intense heat waves while safeguarding vulnerable populations. These insights form a foundational basis for informed policy-making and adaptive urban planning to bolster resilience against intensifying climate risks.

Fig. 15 presents the spatial distribution of projected HWR levels in Bologna for the year 2050, modeled using the developed LSTM under three RCP scenarios. The maps reveal a marked expansion of areas classified as 'High' and 'Very High' risk, particularly under the more extreme emission scenarios. These projections provide critical spatial insights, helping to identify vulnerable census tracts where targeted adaptation and mitigation strategies will be most urgently needed.

The spatial analysis of projected 'Medium' and 'High' risk areas (Fig. 10d and Fig. 15) reveals distinct geographic patterns concentrated in central and southern Bologna. These areas are characterized by a high frequency of historical heatwave events, confirmed by temperature anomaly records during the summers of 2017, 2019, and 2022. Population agglomeration is another critical factor. These zones contain densely inhabited residential blocks with a significant proportion of elderly individuals living alone. Furthermore, these high-risk tracts generally exhibit reduced green space coverage and poor accessibility to vegetated areas. As highlighted in Fig. 13, PDPs show that increasing distance to green areas and lower EVI values are strongly correlated with elevated HWR, underlining the importance of ecological infrastructure. The strength of our spatio-temporal ML-based framework lies in its ability to detect such spatial patterns and their latent drivers. By integrating LSTM's temporal learning capacity with spatially explicit indicators, the model effectively captures non-linear interactions across space and time. This enables not just classification but a form of spatial causal inference, where spatial features (e.g., proximity to cooling infrastructure) can be quantitatively linked to risk levels.

4.8. Influence of green infrastructure on heat wave risk

The development of green space systems has been shown to effectively mitigate heat wave impacts, alleviate the UHI effect, and support health and well-being of residents (Kabisch et al., 2016). Parks, gardens, and urban forests significantly cool ambient temperatures through evapotranspiration and shade, making the integration of green spaces into urban planning a crucial strategy for building climate resilience. This approach addresses both the immediate effects of extreme heat and supports long-term mental and physical health in urban populations.

- **Distance to greenery:** the developed model demonstrates that proximity to green areas significantly influences HWR categories ('High' and 'Very High'). As summarized in Table 6, enhancing proximity to greenery, reducing distance by 2.5 % to 15 %, consistently reduces HWR across all RCP scenarios. The APC results prove the HWR decrease of −6.07 % for RCP 4.5, −6.01 % for RCP 6.0, and −8.01 % for RCP 8.5, highlighting the vital role of increased urban greenery in mitigating heat wave impacts. The most substantial reductions occur under RCP 8.5, indicating a higher sensitivity of HWRs to urban greenery in more severe climate scenarios. This trend emphasizes the importance of strategically enhancing green space proximity in densely populated areas to strengthen urban resilience against heat waves.

- **Vegetation index:** the relationship between EVI improvements and urban cooling is intricate, requiring advanced analytical methods like ML models to discern their detailed impacts. Our findings, detailed in Table 7, reveal that those enhancements in vegetation quality and density lead to notable reductions in HWR across various RCP scenarios. For example, in the RCP 4.5 scenario, a 2.5 % increase in EVI results in a 0.52 % decrease in HWR, with further reductions reaching up to 5.62 % as EVI increases by 15 %, averaging APC of −3.62 %. The trend is similar under RCP 6.0, though slightly less pronounced, with reductions stabilizing around −3.62 % for a 15 % EVI increase, and an APC of −2.79 %. RCP 8.5 shows the greatest sensitivity to EVI enhancements, starting with a 0.93 % risk reduction at a 2.5 % increase and escalating to a 7.62 % decrease at a 15 % improvement, with an APC of −4.74 %.

Fig. 16 illustrates the boxplots distribution of changes in HWR across varying levels of reduced distance to greenery and vegetation index under three RCP scenarios. Each box represents the interquartile range (IQR), with the median line indicating the central tendency of HWR reduction. Narrower boxes suggest lower variability, while wider boxes indicate more uncertainty in the model's response. The results show that under RCP 8.5, reductions in both distance to greenery and vegetation loss yield stronger and more variable HWR decreases, emphasizing the critical role of green infrastructure in high-emission futures. The results indicate that greater proximity to greenery consistently leads to a reduction in HWR, with the most substantial median and IQR range observed under RCP 8.5. Similarly, improvements in the vegetation index are associated with notable decreases in HWR, particularly under higher-emission scenarios. These findings suggest that enhancing access to green infrastructure, both in terms of spatial proximity and vegetation density, is especially critical in high-emission futures, where heat wave intensity and frequency are expected to escalate.

While this section highlights the importance of vegetation and green spaces in mitigating HWR, it is important to note that such NBSs are not the only strategies available. Urban morphology, as characterized by LCZs, also plays a critical role in shaping microclimatic conditions and thermal exposure. LCZs reflect key physical attributes such as building height, spacing, surface cover, and imperviousness, which influence heat storage, ventilation, and radiation balance. Therefore, in addition to enhancing green infrastructure, urban planning interventions that modify built form such as increasing surface albedo, reducing building density, or promoting ventilation corridors can also contribute meaningfully to long-term HWR reduction. Although the LCZs in this study are considered static, their inclusion provides a structural foundation for evaluating morphological adaptations in future assessments.

4.9. Practical considerations

This study presents a data-driven framework for assessing and mitigating urban HWR, enhancing urban resilience. By integrating LSTM with the HOA and employing interpretable risk mapping, it supports adaptive urban planning, informs public health strategies, and promotes NBSs like green infrastructure to reduce vulnerability to climate-related hazards.

Our findings reveal that high-risk zones often coincide with areas of social vulnerability. These include elderly, socially isolated, or foreign-born populations, as well as limited access to green infrastructure. By incorporating fine-scale demographic indicators alongside environmental variables, the model captures critical socio-environmental

Table 5
Comparison of observed HWR levels in 2023 and projected levels for 2050 under RCP 4.5, RCP 6.0, and RCP 8.5 scenarios.

Heat wave Risk Level	Frequency			
	Observed HWR (Year 2023)		Projected HWR (Year 2050)	
	Actual	RCP 4.5	RCP 6.0	RCP 8.5
Very low	0.30	0.17	0.16	0.13
Low	0.15	0.12	0.08	0.08
Moderate	0.12	0.11	0.11	0.08
High	0.09	0.09	0.11	0.05
Very high	0.34	0.51	0.54	0.66

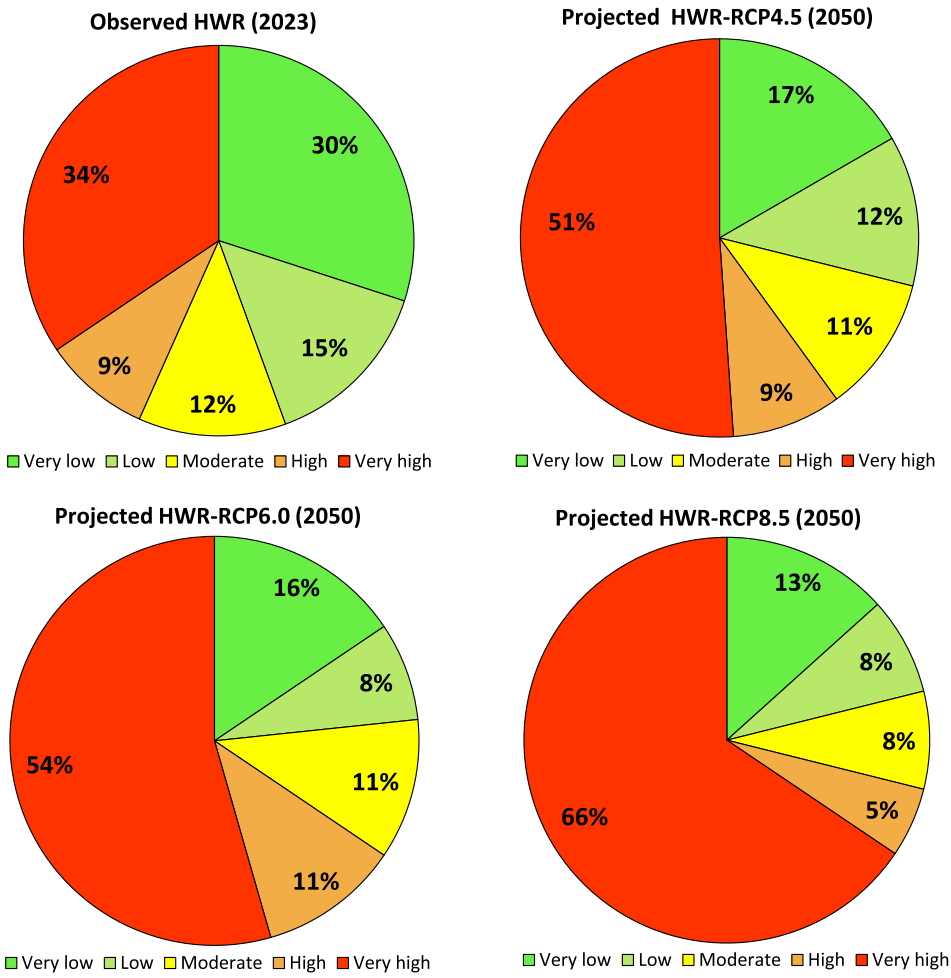

Fig. 14. Observed HWR levels in 2023 V.S. projected HWR levels in 2050 under RCP 4.5, RCP 6.0, and RCP 8.5 scenarios in Bologna.

disparities in heatwave exposure. The importance of healthcare and transit proximity, highlighted through PDP analysis, reinforces the need for integrated adaptation strategies such as cooling shelters and green space investments to support equitable resilience planning in Bologna.

The generated HWR maps offer a practical tool for guiding urban adaptation in Bologna. By identifying neighborhoods with high thermal exposure and social vulnerability, the model supports targeted deployment of NBSs such as tree planting, green roofs, green walls, and shaded parks. These strategies should be prioritized in high-risk areas, particularly those housing elderly or socially isolated populations, to maximize cooling benefits and public health protection. Empirical studies underscore the effectiveness of such measures. Green infrastructure has been shown to reduce extreme heat hours by up to 64.5 % and surface runoff by 58 % (Pace et al., 2025). Green roofs and walls significantly lower surface and indoor temperatures (Ávila-Hernández et al., 2023), while dense tree canopies can reduce surface temperatures by 4 °C per unit increase in Leaf Area Index (Rahman et al., 2020). Urban parks larger than 10 hectares provide notable cooling benefits in terms of both distance and intensity (Aram et al., 2019). Importantly, the effectiveness of NBS depends on local design, vegetation type, and integration with existing infrastructure (Debele et al., 2019; Heymans et al., 2019). Therefore, interventions in Bologna must be tailored to its Mediterranean climate and urban fabric. By aligning spatial risk patterns with targeted adaptation strategies, our framework supports the goals outlined in Bologna's SECAP and the Piano del Verde. It provides urban planners and decision-makers with an evidence-based foundation for equitable resource allocation, thermal comfort enhancement, and public health protection.

5. Limitations and future direction

This study presents a robust LSTM-HOA framework for HWR assessment in Bologna, yet several limitations remain. First, restricted access to high-resolution health and demographic data limited the analysis of individual-level vulnerability, especially among the older population. Incorporating hospital admissions and mortality data could enhance future models. The population exposure was assessed based on static census-based population data. While this provides a foundational view of spatial exposure, it does not capture the dynamic nature of population movements, such as commuting flows or daily activity patterns. Due to the unavailability of high-resolution spatiotemporal mobility data for Bologna, dynamic exposure could not be integrated into the current model. Future studies should aim to incorporate mobility data, including commuting and migration patterns, to enhance the accuracy and validity of exposure assessment in urban HWR analyses. This is particularly important during the summer months, when older populations often travel to nearby coastal regions such as Ravenna and Rimini, potentially altering their exposure to HWR.

Second, while the analysis accounts for varying levels of exposure and demographic vulnerability, it does not capture the full complexity of how heat waves affect human health. Factors such as time spent indoors versus outdoors, occupational exposure, access to cooling resources, and the influence of medications or pre-existing conditions were not considered, yet they may significantly modulate risk. Instead, we relied

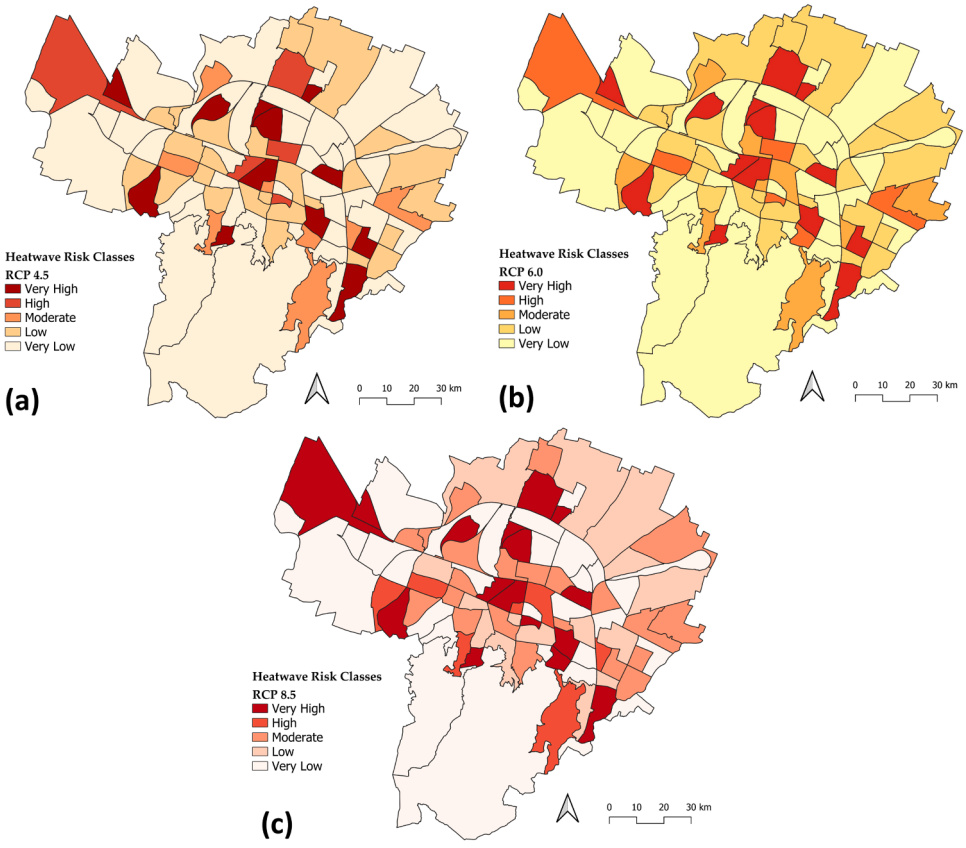

Fig. 15. Spatial distribution of projected HWR levels in 2050 under different RCP scenarios using the developed LSTM model: a) RCP 4.5, b) RCP 6.0, c) RCP 8.5.

Table 6
Impact of reduced distance to greenery on the variation of HWR under future climate scenarios (RCP 4.5, RCP 6.0, and RCP 8.5),.

Scenario	Variation of Distance to Greenery (in %)						APC
	−2.5 %	−5.0 %	−7.5 %	−10.0 %	−12.5 %	−15.0 %	
RCP 4.5	−1.25 %	−2.75 %	−3.95 %	−5.84 %	−5.94 %	−6.07 %	−4.30 %
RCP 6.0	−1.05 %	−1.92 %	−2.32 %	−3.62 %	−5.41 %	−6.01 %	−3.46 %
RCP 8.5	−1.72 %	−2.94 %	−4.06 %	−7.13 %	−7.92 %	−8.01 %	−5.29 %

Table 7
Impact of vegetation index on the variation of HWR under future climate scenarios (RCP 4.5, RCP 6.0, and RCP 8.5).

Scenario	Variation percentage of EVI						APC
	+2.5 %	+5.0 %	+7.5 %	+10.0 %	+12.5 %	+15.0 %	
RCP 4.5	−0. 52 %	−1.94 %	−3.64 %	−4.71 %	−5.31 %	−5.62 %	−3.62 %
RCP 6.0	−0.47 %	−1.51 %	−2.12 %	−4.40 %	−3.31 %	−3.62 %	−2.79 %
RCP 8.5	−0.93 %	−2.97 %	−4.87 %	−5.71 %	−6.31 %	−7.62 %	−4.74 %

on widely accepted proxies, including demographic indicators (e.g., proportion of elderly population), built environment characteristics (e.g., LCZs), and population density, which are commonly used in urban heat risk studies. While these proxies provide a meaningful approximation of population vulnerability, we recognize that they do not fully substitute for health-tied impact data. Future studies may benefit from integrating health surveillance or hospitalization records to further strengthen model validation and improve the assessment of human health impacts associated with heat waves.

Third, the model is tailored to Bologna's urban and climatic context; its application to other cities requires regional calibration. Additionally, while the study highlights the importance of green infrastructure, it does not quantify the dynamic evolution or maintenance of such spaces over time. The long-term effectiveness of NBSs, such as urban greening, in reducing HWR under evolving urban growth and climate scenarios remains untested.

Afterwards, to further strengthen the evaluation of model robustness, future work should consider benchmarking the proposed LSTM-Hippopotamus model against non-optimized LSTM and traditional machine learning classifiers, as well as conducting ablation studies to assess the contribution of individual components. Moreover, tools from the field of explainable AI such as SHAP (SHapley Additive exPlanations) could enhance model interpretability and provide more granular insight into feature importance. Evaluating the model's performance on unseen datasets across different temporal or spatial contexts is also recommended to better assess generalizability under varying input conditions.

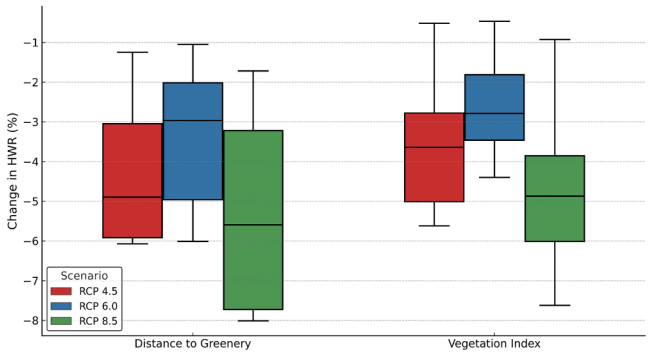

Fig. 16. Variation in HWR as a function of proximity to greenery and vegetation index under different climate scenarios (RCP 4.5, RCP 6.0, and RCP 8.5).

Finally, although the model offers strong predictive performance and interpretability, its integration into practical planning tools such as early warning systems or urban resilience dashboards is a critical next step. Future work should focus on broader data access, cross-city validation, and the co-development of interactive platforms with urban planners to translate model insights into actionable strategies.

5.1. Summary and conclusions

This study presents a novel framework for assessing Heat Wave Risk (HWR) in Bologna, focusing on the older population as a highly vulnerable group, using a Long Short-Term Memory (LSTM) neural network optimized via the Hippopotamus Optimization Algorithm (HOA). By integrating 14 spatial and temporal variables spanning hazard, exposure, and vulnerability components, we offer a robust spatio-temporal ML-based approach to predict and map HWR in Bologna, Italy. The main findings can be summarized as follows:

- The developed LSTM-HOA model achieved strong classification performance across five HWR categories, with class-wise accuracies exceeding 77 % for 'Very Low' and 'High' risk classes. While class-wise disparities were observed, the overall accuracy and stability confirmed the model's suitability for spatial risk mapping at the census tract level.
- Feature selection analyses identified temperature, Local Climate Zones (LCZs), proximity to public transport, and Enhanced Vegetation Index (EVI) as critical contributors to HWR. Notably, areas with higher temperatures, limited vegetation, and poor access to green spaces and transportation exhibited elevated risk levels, particularly for older population residents.
- The use of Partial Dependence Plots (PDPs) improved the explainability of the LSTM model, revealing nonlinear and threshold-based relationships. High temperatures (>29 °C), low EVI (<1000), and greater distances to healthcare and green infrastructure significantly elevated predicted risk, underscoring the need for proximity-based interventions.
- Future risk projections under Representative Concentration Pathways (RCPs) 4.5, 6.0, and 8.5 indicate a substantial increase in 'Very High' risk zones by 2050, with worst-case scenarios showing a rise from 34 % to 66 %. These trends highlight the pressing need for Nature-Based Solutions (NBSs), especially green infrastructure, to buffer urban populations from escalating heat wave hazards.
- Simulation of greenery proximity and vegetation enhancement scenarios demonstrated measurable reductions in projected risk, up to 8 % under RCP 8.5, proving tangible benefits of urban greening in climate adaptation strategies.

We recommend that future studies expand this framework to other cities and incorporate real-time health data and Internet of Things (IoT)-based monitoring systems to enhance model responsiveness. The proposed methodology, due to its interpretability, spatial precision, and predictive strength, suggests the benefit of localized strategies and offers a valuable decision-support tool for urban planners, public health officials, and policymakers in designing climate-resilient and equitable urban environments.

CRediT authorship contribution statement

Aniseh Saber: Writing – original draft, Visualization, Validation, Software, Methodology, Investigation, Formal analysis, Data curation, Conceptualization. **Claudia De Luca:** Writing – original draft, Supervision, Resources, Project administration, Funding acquisition, Conceptualization. **Ali Pourzangbar:** Writing – original draft, Visualization, Software, Methodology, Investigation, Formal analysis, Data curation, Conceptualization. **Simona Tondelli:** Supervision, Resources, Project administration, Funding acquisition, Conceptualization. **Michelle L. Bell:** Supervision, Project administration, Methodology, Investigation, Conceptualization.

Declaration of competing interest

The authors declare that they have no known competing financial interests or personal relationships that could have appeared to influence the work reported in this paper.

Acknowledgments

This research was funded by Doctoral scholarship from the National Operational Programme for Research and Innovation 2014–2020 (CCI 2014IT16M2OP005), FSE REACT-EU funds, Action IV.4 "Doctorates and research contracts on innovation themes" and Action IV.5 "Doctorates on Green themes" (J35F21002810006).

Borsa di dottorato del Programma Operativo Nazionale Ricerca e Innovazione 2014–2020 (CCI 2014IT16M2OP005), risorse FSE REACT-EU, Azione IV.4 "Dottorati e contratti di ricerca su tematiche dell'innovazione" e Azione IV.5 "Dottorati su tematiche Green" (J35F21002810006).

Data availability

Data will be made available on request.

References

Adams, R. M., Evans, C., Wolkin, A., Thomas, T., & Peek, L. (2022). Social vulnerability and disasters: Development and evaluation of a CONVERGE training module for researchers and practitioners. Disaster Prevention and Management. *An International Journal, 31*. https://doi.org/10.1108/DPM-04-2021-0131

Ahmadlou, M., Ghajari, Y. E., & Karimi, M. (2022). Enhanced classification and regression tree (CART) by genetic algorithm (GA) and grid search (GS) for flood susceptibility mapping and assessment. *Geocarto International, 37*. https://doi.org/10.1080/10106049.2022.2082550

Aksangür, İ., Eren, B., & Erden, C. (2022). Evaluation of data preprocessing and feature selection process for prediction of hourly PM10 concentration using long short-term memory models. *Environmental Pollution, 311*. https://doi.org/10.1016/j.envpol.2022.119973

Amiri, M. H., Mehrabi Hashjin, N., Montazeri, M., Mirjalili, S., & Khodadadi, N. (2024). Hippopotamus optimization algorithm: A novel nature-inspired optimization algorithm. *Scientific Reports, 14*. https://doi.org/10.1038/s41598-024-54910-3

Anderson, G. B., & Bell, M. L. (2011). Heat waves in the United States: Mortality risk during heat waves and effect modification by heat wave characteristics in 43 US. communities. *Environ Health Perspect, 119*. https://doi.org/10.1289/ehp.1002313

Aram, F., Higueras García, E., Solgi, E., & Mansournia, S. (2019). Urban green space cooling effect in cities. *Heliyon*. https://doi.org/10.1016/j.heliyon.2019.e01339

Aubrecht, C., & Özceylan, D. (2013). Identification of heat risk patterns in the U.S. National Capital Region by integrating heat stress and related vulnerability. *Environment International, 56*. https://doi.org/10.1016/j.envint.2013.03.005

Ávila-Hernández, A., Simá, E., & Ché-Pan, M. (2023). Research and development of green roofs and green walls in Mexico: A review. *Science of the Total Environment*. https://doi.org/10.1016/j.scitotenv.2022.158978

Ayala-Azcárraga, C., Diaz, D., & Zambrano, L. (2019). Characteristics of urban parks and their relation to user well-being. *Landscape and Urban Planning, 189*. https://doi.org/10.1016/j.landurbplan.2019.04.005

Aydin, H. E., & Iban, M. C. (2023). Predicting and analyzing flood susceptibility using boosting-based ensemble machine learning algorithms with SHapley Additive exPlanations. *Natural Hazards, 116*. https://doi.org/10.1007/s11069-022-05793-y

Bach, S., Binder, A., Montavon, G., Klauschen, F., Müller, K. R., & Samek, W. (2015). On pixel-wise explanations for non-linear classifier decisions by layer-wise relevance propagation. *PLoS One, 10*. https://doi.org/10.1371/journal.pone.0130140

Ballester, J., Quijal-Zamorano, M., Turrubiates, R. F. M., Pegenaute, F., Herrmann, F. R., Robine, J. M., Basagaña, X., Tonne, C., Antó, J. M., & Achebak, H. (2023). Heat-related mortality in Europe during the summer of 2022. *Nature Medicine, 29*. https://doi.org/10.1038/s41591-023-02419-z

Becker, F. N., Fink, A. H., Bissolli, P., & Pinto, J. G. (2022). Towards a more comprehensive assessment of the intensity of historical European heat waves (1979–2019). *Atmospheric Science Letters, 23*. https://doi.org/10.1002/asl.1120

Bell, M. L., O'Neill, M. S., Ranjit, N., Borja-Aburto, V. H., Cifuentes, L. A., & Gouveia, N. C. (2008). Vulnerability to heat-related mortality in Latin America: A case-crossover study in São Paulo, Brazil, Santiago, Chile and Mexico City, Mexico. *International Journal of Epidemiology, 37*. https://doi.org/10.1093/ije/dyn094

Bowler, D. E., Buyung-Ali, L., Knight, T. M., & Pullin, A. S. (2010). Urban greening to cool towns and cities: A systematic review of the empirical evidence. *Landscape and Urban Planning*. https://doi.org/10.1016/j.landurbplan.2010.05.006

Bradford, K., Abrahams, L., Hegglin, M., & Klima, K. (2015). A heat vulnerability index and adaptation solutions for Pittsburgh, Pennsylvania. *Environ Sci Technol, 49*. https://doi.org/10.1021/acs.est.5b03127

Byagar, S., Deshmukh, A. A., Wanjale, K., Wadne, V. S., Ranjan, N., & Gangarde, R. (2024). Heat wave prediction using recurrent neural networks based on deep learning. *International Journal of Intelligent Systems and Applications in Engineering, 12*.

C40 Cities. (2016). *The compact of mayors [WWW document]*. C40 Cities. https://www.c40.org/what-we-do/initiatives/compact-of-mayors/ accessed 6.12.25.

Chausson, A., Turner, B., Seddon, D., Chabaneix, N., Girardin, C. A. J., Kapos, V., Key, I., Roe, D., Smith, A., Woroniecki, S., & Seddon, N. (2020). Mapping the effectiveness of nature-based solutions for climate change adaptation. *Global Change Biology, 26*. https://doi.org/10.1111/gcb.15310

Chung, J., Lee, Y., Jang, W., Lee, S., & Kim, S. (2020). Correlation analysis between air temperature and MODIS land surface temperature and prediction of air temperature using tensorflow long short-term memory for the period of occurrence of cold and heat waves. *Remote Sensing*, 12. https://doi.org/10.3390/rs12193231

Cianconi, P., Betrò, S., & Janiri, L. (2020). The impact of climate change on mental health: A systematic descriptive review. *Frontiers in Psychiatry, 11*. https://doi.org/10.3389/fpsyt.2020.00074

Copernicus Climate Change Service, C.D.S., 2023. ERA5 hourly data on single levels from 1940 to present. Copernicus Climate Change service (C3S) Climate Data Store (CDS) [WWW Document]. 2023. https://doi.org/10.24381/cds.adbb2d47 (accessed 6.12.25).

Côté, J. N., Germain, M., Levac, E., & Lavigne, E. (2024). Vulnerability assessment of heat waves within a risk framework using artificial intelligence. *Science of the Total Environment, 912*. https://doi.org/10.1016/j.scitotenv.2023.169355

Cremonini, L., Georgiadis, T., Nardino, M., Rossi, F., Rossi, A., Pinca, G., & Fazzini, M. (2023). Tools for Urban climate Adaptation Plans: A case study on Bologna and outcomes for heat wave impact reduction. *Challenges, 14*. https://doi.org/10.3390/challe14040048

Debele, S. E., Kumar, P., Sahani, J., Marti-Cardona, B., Mickovski, S. B., Leo, L. S., Porcù, F., Bertini, F., Montesi, D., Vojinovic, Z., & Di Sabatino, S. (2019). Nature-based solutions for hydro-meteorological hazards: Revised concepts, classification schemes and databases. *Environmental Resarch*. https://doi.org/10.1016/j.envres.2019.108799

Dhake, H., Kashyap, Y., & Kosmopoulos, P. (2023). Algorithms for hyperparameter tuning of LSTMs for time series forecasting. *Remote Sensing*, 15. https://doi.org/10.3390/rs15082076

EEA. (2023). *Europe's air quality status 2023 [WWW document]*. European Environment Agency. https://www.eea.europa.eu/publications/europes-air-quality-status-2023 accessed 6.12.25.

Ellena, M., Melis, G., Zengarini, N., Gangi, E. Di, Ricciardi, G., Mercogliano, P., & Costa, G. (2023). Micro-scale UHI risk assessment on the heat-health nexus within cities by looking at socio-economic factors and built environment characteristics: The Turin case study (Italy). *Urban Climate*, 49. https://doi.org/10.1016/j.uclim.2023.101514

Fisher, R.A., 1992. Statistical methods for research workers. https://doi.org/10.1007/978-1-4612-4380-9_6.

Gao, Z., Hou, Y., & Chen, W. (2019). Enhanced sensitivity of the urban heat island effect to summer temperatures induced by urban expansion. *Environmental Research Letters, 14*. https://doi.org/10.1088/1748-9326/ab2740

García-Nieto, P. J., García-Gonzalo, E., & Paredes-Sánchez, J. P. (2021). Prediction of the critical temperature of a superconductor by using the WOA/MARS, Ridge, Lasso and Elastic-net machine learning techniques. *Neural Computing & Applications, 33*. https://doi.org/10.1007/s00521-021-06304-z

Gasparrini, A., Guo, Y., Hashizume, M., Lavigne, E., Zanobetti, A., Schwartz, J., Tobias, A., Tong, S., Rocklöv, J., Forsberg, B., Leone, M., De Sario, M., Bell, M. L., Guo, Y. L. L., Wu, C. F., Kan, H., Yi, S. M., De Sousa Zanotti Stagliorio Coelho, M., Saldiva, P. H. N., Honda, Y., Kim, H., & Armstrong, B. (2015). Mortality risk attributable to high and low ambient temperature: A multicountry observational study. *The Lancet, 386*. https://doi.org/10.1016/S0140-6736(14)62114-0

Ghafarian, F., Wieland, R., Lüttschwager, D., & Nendel, C. (2022). Application of extreme gradient boosting and Shapley Additive explanations to predict temperature regimes inside forests from standard open-field meteorological data. *Environmental Modelling and Software, 156*. https://doi.org/10.1016/j.envsoft.2022.105466

Gordon, T. J., & Glenn, J. C. (2003). *Futures research methodology. millennium project of the*. American Council for the United Nations University.

Gronlund, C. J., Berrocal, V. J., White-Newsome, J. L., Conlon, K. C., & O'Neill, M. S. (2015). Vulnerability to extreme heat by socio-demographic characteristics and area green space among the elderly in Michigan, 1990-2007. *Environmental Resarch, 136*. https://doi.org/10.1016/j.envres.2014.08.042

Gunes, T. (2023). Model agnostic interpretable machine learning for residential property valuation. *Survey Review*. https://doi.org/10.1080/00396265.2023.2293366

Hair, F. J., Black, C., W., Babin, J. B., & Anderson, E. R. (2019). Multivariate Data analysis. *E-Jurnal Manajemen Universitas Udayana, 5*.

Han, J., & Vartosh, A. (2023). Multi-objective grasshopper optimization algorithm for optimal energy scheduling by considering heat as integrated demand response. *Applied Thermal Engineering, 234*. https://doi.org/10.1016/j.applthermaleng.2023.121242

Hass, A. L., & Ellis, K. N. (2019). Using wearable sensors to assess how a heatwave affects individual heat exposure, perceptions, and adaption methods. *International Journal Of Biometeorology, 63*. https://doi.org/10.1007/s00484-019-01770-6

Heymans, A., Breadsell, J., Morrison, G. M., Byrne, J. J., & Eon, C. (2019). Ecological urban planning and design: A systematic literature review. *Sustainability (Switzerland)*. https://doi.org/10.3390/su11133723

IPCC. (2023). In H. Lee, & J. Romero (Eds.), *Climate change 2023: Synthesis report. contribution of working groups I, II and III to the sixth assessment report of the intergovernmental panel on climate change [Core writing team*. Geneva, Switzerland: IPCC.

IPCC. (2014a). In C. B. Field, V. R. Barros, D. J. Dokken, K. J. Mach, M. D. Mastrandrea, T. E. Bilir, M. Chatterjee, K. L. Ebi, Y. O. Estrada, R. C. Genova, B. Girma, E. S. Kissel, A. N. Levy, S. MacCracken, P. R. Mastrandrea, & L. L. White (Eds.), *Climate change 2014: Impacts, adaptation, and vulnerability. part A: Global and sectoral aspects. contribution of working group ii to the fifth assessment report of the intergovernmental panel on climate change*. United Kingdom and New York, NY, USA: Cambridge.

IPCC. (2014b). *Climate change 2014: Impacts, adaptation, and vulnerability. part A: Global and sectoral aspects*. Cambridge, United Kingdom and New York, NY, USA: Cambridge University Press.

ISTAT, 2024. Demo: Demographics in numbers [WWW Document]. https://demo.istat.it/(accessed 6.11.25).

Jacques-Dumas, V., Ragone, F., Borgnat, P., Abry, P., & Bouchet, F. (2022). Deep learning-based extreme heatwave forecast. *Frontiers in Climate, 4*. https://doi.org/10.3389/fclim.2022.789641

Jamil, M. A., & Khanam, S. (2024). Influence of one-way ANOVA and Kruskal–Wallis based feature ranking on the performance of ML classifiers for bearing fault diagnosis. *Journal of Vibration Engineering and Technologies, 12*. https://doi.org/10.1007/s42417-023-01036-x

Jenks, G. F. (1963). Generalization in statistical mapping. *Annals of the Association of American Geographers, 53*. https://doi.org/10.1111/j.1467-8306.1963.tb00429.x

Joe, P., Baklanov, A., Grimmond, S., Bouchet, V., Molina, L. T., Schluenzen, K. H., Mills, G., Tan, J., Golding, B., Masson, V., Ren, C., Voogt, J., Miao, S., Lean, H., Heusinkveld, B., Hovespyan, A., Terrugi, G., Parrish, P., Christensen, J. H., Fallmann, J., Sokhi, R., Spengler, R., & Yoshitani, J. (2021). Guidance on integrated urban hydro-meteorological, Climate and environmental services: Challenges and the way forward. *Biometeorology*. https://doi.org/10.1007/978-3-030-87598-5_14

Kabisch, N., Frantzeskaki, N., Pauleit, S., Naumann, S., Davis, M., Artmann, M., Haase, D., Knapp, S., Korn, H., Stadler, J., Zaunberger, K., & Bonn, A. (2016). Nature-based solutions to climate change mitigation and adaptation in urban areas: Perspectives on indicators, knowledge gaps, barriers, and opportunities for action. *Ecology and Society, 21*. https://doi.org/10.5751/ES-08373-210239

Karimi, A., Mohajerani, M., Alinasab, N., & Akhlaghinezhad, F. (2024). Integrating machine learning and genetic algorithms to optimize building energy and thermal efficiency under historical and future climate scenarios. *Sustainability*, 16.

Karner, A. (2018). Assessing public transit service equity using route-level accessibility measures and public data. *Journal of Transport Geography, 67*. https://doi.org/10.1016/j.jtrangeo.2018.01.005

Khan, N., Shahid, S., Ismail, T. Bin, & Behlil, F. (2021). Prediction of heat waves over Pakistan using support vector machine algorithm in the context of climate change. *Stochastic Environmental Research and Risk Assessment, 35*. https://doi.org/10.1007/s00477-020-01963-1

Kim, D. W., Deo, R. C., Lee, J. S., & Yeom, J. M. (2017). Mapping heatwave vulnerability in Korea. *Natural Hazards, 89*. https://doi.org/10.1007/s11069-017-2951-y

Kottek, M., Grieser, J., Beck, C., Rudolf, B., & Rubel, F. (2006). World map of the Köppen-Geiger climate classification updated. *Meteorologische Zeitschrift, 15*. https://doi.org/10.1127/0941-2948/2006/0130

Kruskal, W. H., & Wallis, W. A. (1952). Use of ranks in one-criterion variance analysis. *Journal of the American Statistical Association, 47*. https://doi.org/10.1080/01621459.1952.10483441

Kudela, J., & Matousek, R. (2022). New benchmark functions for single-objective optimization based on a zigzag pattern. *IEEE access : Practical Innovations, Open Solutions, 10*. https://doi.org/10.1109/ACCESS.2022.3144067

Kumar, N., Poonia, V., Gupta, B. B., & Goyal, M. K. (2021). A novel framework for risk assessment and resilience of critical infrastructure towards climate change. *Technological Forecasting And Social Change, 165*. https://doi.org/10.1016/j.techfore.2020.120532

Kumar, S., Pal, S. K., & Singh, R. (2019). A novel hybrid model based on particle swarm optimisation and extreme learning machine for short-term temperature prediction using ambient sensors. *Sustainable Cities and Society, 49*. https://doi.org/10.1016/j.scs.2019.101601

Labib, S. M., Lindley, S., & Huck, J. J. (2020). Spatial dimensions of the influence of urban green-blue spaces on human health: A systematic review. *Environmental Research*. https://doi.org/10.1016/j.envres.2019.108869

Lhotka, O., & Kyselý, J. (2022). The 2021 European heat wave in the context of past major heat waves. *Earth and Space Science, 9*. https://doi.org/10.1029/2022EA002567

LIFEGATE. (2023). *Come bologna è diventata la città più resiliente d'Italia [WWW document]*. LIFEGATE.

Marando, F., Heris, M. P., Zulian, G., Udías, A., Mentaschi, L., Chrysoulakis, N., Parastatidis, D., & Maes, J. (2022). Urban heat island mitigation by green infrastructure in European Functional Urban Areas. *Sustainable Cities and Society, 77*. https://doi.org/10.1016/j.scs.2021.103564

McCarthy, M., Armstrong, L., & Armstrong, N. (2019). A new heatwave definition for the UK. *Weather, 74*. https://doi.org/10.1002/wea.3629

Messeri, A., Morabito, M., Bonafede, M., Bugani, M., Levi, M., Baldasseroni, A., Binazzi, A., Gozzini, B., Orlandini, S., Nybo, L., & Marinaccio, A. (2019). Heat stress perception among native and migrant workers in italian industries—Case studies from the construction and agricultural sectors. *International Journal Of Environmental Research And Public Health, 16*. https://doi.org/10.3390/ijerph16071090

Moosbauer, J., Herbinger, J., Casalicchio, G., Lindauer, M., & Bischl, B. (2021). Explaining hyperparameter optimization via partial dependence plots. *Advances in neural information processing systems*.

Morabito, M., Crisci, A., Gioli, B., Gualtieri, G., Toscano, P., Stefano, V. Di, Orlandini, S., & Gensini, G. F. (2015). Urban-hazard risk analysis: Mapping of heat-related risks in the elderly in major Italian cities. *PLoS One, 10*. https://doi.org/10.1371/journal.pone.0127277

Mudelsee, M. (2019). Trend analysis of climate time series: A review of methods. *Earth Science Reviews*. https://doi.org/10.1016/j.earscirev.2018.12.005

Nardino, M., Cremonini, L., Crisci, A., Georgiadis, T., Guerri, G., Morabito, M., & Fiorillo, E. (2022). Mapping daytime thermal patterns of Bologna municipality (Italy) during a heatwave: A new methodology for cities adaptation to global climate change. *Urban Climate, 46*. https://doi.org/10.1016/j.uclim.2022.101317

Nur, A. S., Kim, Y. J., & Lee, C. W. (2022). Creation of wildfire susceptibility maps in Plumas National Forest using InSAR coherence, deep learning, and metaheuristic optimization approaches. *Remote sensing*, 14. https://doi.org/10.3390/rs14174416

Pace, R., Endreny, T. A., Ciolfi, M., Gangwisch, M., Saha, S., Ruehr, N. K., & Grote, R. (2025). Mitigation potential of urban greening during heatwaves and stormwater events: A modeling study for Karlsruhe. *Germany Science Reports, 15*, 5308. https://doi.org/10.1038/s41598-025-89842-z

Park, M., Jung, D., Lee, S., & Park, S. (2020). Heatwave damage prediction using random forest model in Korea. *Applied Sciences (Switzerland)*, 10. https://doi.org/10.3390/app10228237

Pavlov-Kagadejev, M., Jovanovic, L., Bacanin, N., Deveci, M., Zivkovic, M., Tuba, M., Strumberger, I., & Pedrycz, W. (2024). Optimizing long-short-term memory models via metaheuristics for decomposition aided wind energy generation forecasting. *Artificial Intelligence Review, 57*. https://doi.org/10.1007/s10462-023-10678-y

Perkins, S. E., Alexander, L. V., & Nairn, J. R. (2012). Increasing frequency, intensity and duration of observed global heatwaves and warm spells. *Geophysical Research Letters, 39*. https://doi.org/10.1029/2012GL053361

Pinto, L. V., Ferreira, C. S. S., Inácio, M., & Pereira, P. (2022). Urban green spaces accessibility in two European cities: Vilnius (Lithuania) and Coimbra (Portugal). *Geography and Sustainability, 3*. https://doi.org/10.1016/j.geosus.2022.03.001

Pourzangbar, A., Brocchini, M., Saber, A., Mahjoobi, J., Mirzaaghasi, M., & Barzegar, M. (2017a). Prediction of scour depth at breakwaters due to non-breaking waves using machine learning approaches. *Applied Ocean Research, 63*. https://doi.org/10.1016/j.apor.2017.01.012

Pourzangbar, A., Jalali, M., & Brocchini, M. (2023a). Machine learning application in modelling marine and coastal phenomena: A critical review. *Frontiers in Environmental Engineering, 2*. https://doi.org/10.3389/fenve.2023.1235557

Pourzangbar, A., Losada, M. A., Saber, A., Ahari, L. R., Larroudé, P., Vaezi, M., & Brocchini, M. (2017b). Prediction of non-breaking wave induced scour depth at the trunk section of breakwaters using Genetic programming and Artificial Neural Networks. *Coastal Engineering, 121*. https://doi.org/10.1016/j.coastaleng.2016.12.008

Pourzangbar, A., Oberle, P., Kron, A., & Franca, M. J. (2025). Analysis of the utilization of machine learning to map flood susceptibility. *Journal of Flood Risk Management*. https://doi.org/10.1111/jfr3.70042

Pourzangbar, A., Oberle, P., Kron, A., & Franca, M. J. (2023b). On the application of machine learning into flood modeling: Data consideration and modeling algorithm. In P. Gourbesville, & G. Caignaert (Eds.), *Advances in hydroinformatics-simhydro 2023*. Springer. https://doi.org/10.1007/978-981-97-4072-7_11.

Qureshi, Md. M. U., Ahmed, A. B., Dulmini, A., Khan, M. M. H., & Rois, R. (2025). Developing a seasonal-adjusted machine-learning-based hybrid timeseries model to forecast heatwave warning. *Scientific Reports, 15*, 8699. https://doi.org/10.1038/s41598-025-93227-7

Raffa, M., Reder, A., Marras, G. F., Mancini, M., Scipione, G., Santini, M., & Mercogliano, P. (2021). VHR-REA_IT dataset: Very high resolution dynamical downscaling of ERA5 reanalysis over Italy by COSMO-CLM. *Data (Basel)*, 6. https://doi.org/10.3390/data6080088

Rahman, M. A., Stratopoulos, L. M. F., Moser-Reischl, A., Zölch, T., Häberle, K. H., Rötzer, T., Pretzsch, H., & Pauleit, S. (2020). Traits of trees for cooling urban heat islands: A meta-analysis. *Building and Environment*. https://doi.org/10.1016/j.buildenv.2019.106606

Rasheed, K., Qayyum, A., Ghaly, M., Al-Fuqaha, A., Razi, A., & Qadir, J. (2022). Explainable, trustworthy, and ethical machine learning for healthcare: A survey. *Computers in Biology and Medicine*. https://doi.org/10.1016/j.compbiomed.2022.106043

Razavi-Termeh, S. V., Pourzangbar, A., Franca, M. J., & Sadeghi, A. (2025). Metaheuristic-driven enhancement of categorical boosting algorithm for flood-prone areas mapping. *International Journal of Applied Earth Observation and Geoinformation, 136*.

Reichstein, M., Camps-Valls, G., Stevens, B., Jung, M., Denzler, J., Carvalhais, N., & Prabhat. (2019). Deep learning and process understanding for data-driven Earth system science. *Nature, 566*. https://doi.org/10.1038/s41586-019-0912-1

Rezaie, F., Panahi, M., Bateni, S. M., Jun, C., Neale, C. M. U., & Lee, S. (2022). Novel hybrid models by coupling support vector regression (SVR) with meta-heuristic algorithms (WOA and GWO) for flood susceptibility mapping. *Natural Hazards, 114*. https://doi.org/10.1007/s11069-022-05424-6

Russo, S., Sillmann, J., & Sterl, A. (2017). Humid heat waves at different warming levels. *Scientific Reports, 7*. https://doi.org/10.1038/s41598-017-07536-7

Sahani, J., Kumar, P., & Debele, S. E. (2024). Assessing demographic and socioeconomic susceptibilities to heatwaves in the Southeastern United Kingdom. *Sustainable Cities and Society, 117*. https://doi.org/10.1016/j.scs.2024.105958

Sarofim, M. C., Saha, S., Hawkins, M. D., Mills, D. M., Hess, J., Horton, R., Kinney, P., Schwartz, J., & Juliana, A. St. (2016). *Ch. 2: Temperature-related death and illness. the impacts of climate change on human health in the united states*. A Scientific Assessment, U.S. Global Change Research Program.

Selvaraju, R. R., Cogswell, M., Das, A., Vedantam, R., Parikh, D., & Batra, D. (2020). Grad-CAM: Visual explanations from deep networks via gradient-based localization. *International Journal Of Computer Vision, 128*. https://doi.org/10.1007/s11263-019-01228-7

Sepp, H., & Jürgen, S. (1997). Long short-term memory. *Neural Computation*.

Shah, F., & Sharifi, A. (2025). Climate models for predicting precipitation and temperature trends in cities: A systematic review. *Sustainable Cities and Society, 120*. https://doi.org/10.1016/j.scs.2025.106171

Smith, T. T., Zaitchik, B. F., & Gohlke, J. M. (2013). Heat waves in the United States: Definitions, patterns and trends. *Climatic Change, 118*. https://doi.org/10.1007/s10584-012-0659-2

Sobolewski, A., Młynarczyk, M., Konarska, M., & Bugajska, J. (2021). The influence of air humidity on human heat stress in a hot environment. *International Journal of Occupational Safety and Ergonomics, 27*. https://doi.org/10.1080/10803548.2019.1699728

Stewart, I. D., & Oke, T. R. (2012). Local climate zones for urban temperature studies. *Bulletin of the American Meteorological Society, 93*. https://doi.org/10.1175/BAMS-D-11-00019.1

Su, M., Zhong, Q., & Peng, H. (2021). Regularized multivariate polynomial regression analysis of the compressive strength of slag-metakaolin geopolymer pastes based on experimental data. *Construction of Building Materials, 303*. https://doi.org/10.1016/j.conbuildmat.2021.124529

Turner, D. D., Mlawer, E. J., Bianchini, G., Cadeddu, M. P., Crewell, S., Delamere, J. S., Knuteson, R. O., Maschwitz, G., Mlynzcak, M., Paine, S., Palchetti, L., & Tobin, D. C. (2012). Ground-based high spectral resolution observations of the entire terrestrial spectrum under extremely dry conditions. *Geophysical Research Letters, 39*. https://doi.org/10.1029/2012GL051542

UNDRR. (2015). *Sendai framework for disaster risk reduction 2015–2030. united nations*. Geneva: United Nations Office for Disaster Risk Reduction.

Varghese, B. M., Barnett, A. G., Hansen, A. L., Bi, P., Nairn, J., Rowett, S., Nitschke, M., Hanson-Easey, S., Heyworth, J. S., Sim, M. R., & Pisaniello, D. L. (2019). Characterising the impact of heatwaves on work-related injuries and illnesses in three Australian cities using a standard heatwave definition- excess Heat Factor (EHF). *Journal of Exposure Science & Environmental Epidemiology, 29*. https://doi.org/10.1038/s41370-019-0138-1

Varquez, A. C. G., Taerakul, J., Renard, F., Alonso, L., Choi, S., Hiroki, R., Ashie, Y., Kumakura, E., Okumura, M., Hanaoka, S., Inagaki, A., & Kanda, M. (2025). High-resolution outdoor heat-risk modeling for city central areas with applications to Tokyo and Lyon. *Sustainable Cities and Society, 125*. https://doi.org/10.1016/j.scs.2025.106344

Vicedo-Cabrera, A. M., de Schrijver, E., Schumacher, D. L., Ragettli, M. S., Fischer, E. M., & Seneviratne, S. I. (2023). The footprint of human-induced climate change on heat-related deaths in the summer of 2022 in Switzerland. *Environmental Research Letters, 18*. https://doi.org/10.1088/1748-9326/ace0d0

Vivo, C. De, Ellena, M., Capozzi, V., Budillon, G., & Mercogliano, P. (2022). Risk assessment framework for Mediterranean airports: A focus on extreme temperatures and precipitations and sea level rise. *Natural Hazards, 111*. https://doi.org/10.1007/s11069-021-05066-0

Wang, P., Tang, J., Sun, X., Wang, S., Wu, J., Dong, X., & Fang, J. (2017). Heat Waves in China: Definitions, leading patterns, and connections to large-scale atmospheric circulation and SSTs. *Journal of Geophysical Research: Atmospheres, 122*. https://doi.org/10.1002/2017JD027180

Wang, S., Sun, Q. C., Huang, X., Tao, Y., Dong, C., Das, S., & Liu, Y. (2023). Health-integrated heat risk assessment in Australian cities. *Environmental Impact Assessment Review, 102*. https://doi.org/10.1016/j.eiar.2023.107176

WMO, W. H. O. (2015). Heatwaves and health: Guidance on warning-system development. In G. R. McGregor, P. Bessemoulin, K. Ebi, & B. Menne (Eds.), *WMO-No. 1142*. World Meteorological Organization & World Health Organization.

Wong, N. H., Tan, C. L., Kolokotsa, D. D., & Takebayashi, H. (2021). Greenery as a mitigation and adaptation strategy to urban heat. *Nature Reviews Earth and Environment*. https://doi.org/10.1038/s43017-020-00129-5

Woodland, L., Ratwatte, P., Phalkey, R., & Gillingham, E. L. (2023a). Investigating the health impacts of climate change among people with pre-existing mental health

problems: A scoping review. *International Journal Of Environmental Research And Public Health, 20*. https://doi.org/10.3390/ijerph20085563

Woodland, L., Ratwatte, P., Phalkey, R., & Gillingham, E. L. (2023b). Investigating the health impacts of climate change among people with pre-existing mental health problems: A scoping review. *International Journal Of Environmental Research And Public Health, 20*. https://doi.org/10.3390/ijerph20085563

Wu, H., Xu, Y., Zhang, M., Su, L., Wang, Y., & Zhu, S. (2024). Spatially explicit assessment of the heat-related health risk in the Yangtze River Delta, China, using multisource remote sensing and socioeconomic data. *Sustainable Cities and Society, 104*. https://doi.org/10.1016/j.scs.2024.105300

Yadav, H., & Thakkar, A. (2024). NOA-LSTM: An efficient LSTM cell architecture for time series forecasting. *Expert Systems With Applications, 238*. https://doi.org/10.1016/j.eswa.2023.122333

Yang, H., Lee, T., & Juhola, S. (2021). The old and the climate adaptation: Climate justice, risks, and urban adaptation plan. *Sustainable Cities and Society, 67*. https://doi.org/10.1016/j.scs.2021.102755

Ye, J., & Yang, F. (2025). Towards multi-scale and context-specific heat health risk assessment - A systematic review. *Sustainable Cities and Society*. https://doi.org/10.1016/j.scs.2024.106102

Zeng, Z., Zhang, W., Sun, K., Wei, M., & Hong, T. (2022). Investigation of pre-cooling as a recommended measure to improve residential buildings' thermal resilience during heat waves. *Building and Environment, 210*. https://doi.org/10.1016/j.buildenv.2021.108694